AGU PUBLICATIONS

JGR

Journal of Geophysical Research: Atmospheres

RESEARCH ARTICLE
10.1002/2015JD023893

Key Points:
- First stable isotope analysis of rain from an altitudinal transect in Papua
- Seasonal $\delta^{18}O$ may reflect the temperature in clouds at mean condensation level
- Rainfall $\delta^{18}O$ are more enriched during El Niño than during ENSO-normal periods

Supporting Information:
- Text S1 and Figures S1–S12

Correspondence to:
D. S. Permana, and L. G. Thompson,
permana.5@osu.edu;
donaldi.permana@bmkg.go.id;
thompson.3@osu.edu

Citation:
Permana, D. S., L. G. Thompson, and G. Setyadi (2016), Tropical West Pacific moisture dynamics and climate controls on rainfall isotopic ratios in southern Papua, Indonesia, *J. Geophys. Res. Atmos.*, *121*, 2222–2245, doi:10.1002/2015JD023893.

Received 8 JUL 2015
Accepted 17 FEB 2016
Accepted article online 20 FEB 2016
Published online 14 MAR 2016

Tropical West Pacific moisture dynamics and climate controls on rainfall isotopic ratios in southern Papua, Indonesia

Donaldi S. Permana[1,2], Lonnie G. Thompson[1], and Gesang Setyadi[3]

[1]Byrd Polar and Climate Research Center and School of Earth Sciences, Ohio State University, Columbus, Ohio, USA, [2]Research and Development Center, Indonesian Agency for Meteorology Climatology and Geophysics, Jakarta, Indonesia, [3]Environmental Department, PT Freeport Indonesia, Timika, Indonesia

Abstract Understanding the controls on stable isotopologues of tropical rainfall is critical for paleoclimatic reconstruction from tropical ice core records. The southern Papua region, Indonesia, has a unique climate regime that allows for the evaluation of the influence of precipitation and convective activity on seasonal rainfall $\delta^{18}O$. The influence of the El Niño–Southern Oscillation (ENSO) on interannual rainfall $\delta^{18}O$ variation is also important for paleoclimate reconstruction. Here we present stable isotope analyses of 1332 rain samples collected daily during the period from January 2013 to February 2014 (ENSO-normal) and December 2014 to September 2015 (El Niño) at various elevation stations (9 to 3945 m above sea level) on the southern slope of the central mountain ranges in Papua. The results suggest an altitude effect with an isotopic lapse rate for $\delta^{18}O$ (δD) of −2.4‰/km (−18.2‰/km). The temporal $\delta^{18}O$ variability (daily to interannual) is controlled mostly by regional convective activity rather than local/regional precipitation amount. The intraseasonal $\delta^{18}O$ variation resembles the Madden-Julian Oscillation cycle with major $\delta^{18}O$ depletion events associated with active (wet) phases. Moisture origins, transport pathways, moisture convergence, and raindrop evaporation appear to have no significant seasonal effects on $\delta^{18}O$, leading to the conclusion that condensation temperature controls $\delta^{18}O$ depletion associated with convective activity. Seasonal $\delta^{18}O$ variation is likely associated with atmospheric temperature at the mean condensation level as indicated by the altitude of latent heat release in the troposphere. Rainfall $\delta^{18}O$ (δD) is generally enriched by 1.6‰–2‰ (11‰–15‰) during El Niño than during ENSO-normal periods.

1. Introduction

The stable isotopic content of water has been recognized as a powerful tool for paleoclimate reconstruction. In the tropics, there is an empirical negative relationship between the stable isotope ratios in precipitation and the rainfall amount, which defines the stable isotope "amount effect" [*Dansgaard*, 1964; *Rozanski et al*., 1993; *Gonfiantini et al*., 2001]. On seasonal timescales, the amount effect results in rainfall isotopic values being more depleted during rainy seasons than dry seasons [*Gonfiantini et al*., 2001]. The amount effect in rain has been ascribed to fractionation processes that occur on both local [*Vuille et al*., 2005; *Lee et al*., 2009] and larger spatial scales [*Cobb et al*., 2007; *Risi et al*., 2008a; *Kurita et al*., 2009, 2011; *Fudeyasu et al*., 2011; *Tremoy et al*., 2012; *Moerman et al*., 2013; *Kurita*, 2013]. However, previous studies also have linked rainfall isotopic composition to moisture sources, moisture transport history, and/or prevailing weather patterns [*Rhodes et al*., 2006; *Scholl et al*., 2007, 2009; *Kurita et al*., 2009; *Breitenbach et al*., 2010; *Fudeyasu et al*., 2011; *Crawford et al*., 2013; *Suwarman et al*., 2013; *Windhorst et al*., 2013].

The mechanisms that lead to the observed isotope amount effect are poorly understood. The amount effect has been explained as a consequence of the extent of the rainout process from deep convective clouds in the Intertropical Convergence Zone (ITCZ) [*Rozanski et al*., 1993; *Yoshimura et al*., 2003]. In this scenario, greater rain intensity during storm events results in lower isotopic values while less intense rain storms tend to generate precipitation with more enriched isotopic values. Because heavy water vapor is preferably removed as condensation, the remaining vapor becomes lighter. Thus, subsequent precipitation that forms from a given convective air mass will be more isotopically depleted [*Yoshimura et al*., 2003; *Vuille et al*., 2003]. Alternatively, the amount effect has been interpreted by the direct and indirect effects of unsaturated downdrafts in the convective system [*Risi et al*., 2008a, 2008b]. The direct effect of the unsaturated downdrafts is associated with processes of rainfall reevaporation and equilibration through diffusive exchanges. The indirect effect is referred to as downdraft recycling, which decreases the isotopic ratios of atmospheric water vapor by injecting isotopically depleted vapor from the downdrafts into the subcloud layer which feeds the convective

system [*Risi et al*., 2008b]. A recent study demonstrates that moisture convergence is also the main contributor to the interpretation of the amount effect [*Lee et al*., 2007; *Moore et al*., 2014]. Moreover, *Kurita* [2013] suggested that the rainfall isotopic variation in tropical regions is not directly controlled by the precipitation amount but rather depends on large-scale convective activity, as shown by *Lekshmy et al*. [2014] in southern India during the monsoon season. Recently, upwind regional convective activity during the monsoon season has been identified as the main control of isotopic variation in the southern Tibetan Plateau [*Gao et al*., 2013] and over the tropical Andes [*Samuels-Crow et al*., 2014].

In the tropics, most precipitation falls from high convective clouds during the summer monsoon season, corresponding to intensively deep convection originating from low-pressure systems following the annual movement of the ITCZ. Outgoing longwave radiation (OLR) at the top of the atmosphere is routinely used to locate areas of deep convection and precipitation [*Arkin and Ardanuy*, 1989]. The OLR value represents an integral measurement of the radiative effects from the surface, clouds, and gases in the atmosphere. In general, enhanced deep convection associated with high precipitation is identified by low OLR values ($<$205 W m^{-2}) [*Gu and Zhang*, 2002], while high OLR values ($>$205 W m^{-2}) indicate reduced convection with less precipitation or clear-sky condition. Therefore, on seasonal timescales in the tropics, precipitation amount and OLR values are generally inversely correlated.

Correlations between rainfall isotopic variations and large-scale convective activity have also been reported on intraseasonal timescales in tropical South America [*Vimeux et al*., 2011], Africa [*Risi et al*., 2008a; *Tremoy et al*., 2012], the southern Tibetan Plateau [*Gao et al*., 2013], and Southeast Asia [*Moerman et al*., 2013]. The most prominent mode of intraseasonal variability in the tropics is the Madden-Julian Oscillation (MJO) which has 30–60 day periodicity and is characterized by an eastward propagation of both enhanced and reduced tropical cloud convection across the equatorial Indian Ocean to the western and central Pacific Ocean [*Madden and Julian*, 1972]. *Kurita et al*. [2011] showed that rainfall isotopic variation is associated with the intraseasonal MJO. Moreover, *Moerman et al*. [2013] suggested that the large negative values of rainfall δ^{18}O, indicated by low OLR values, are associated with the wet phases of MJO.

From a different perspective, OLR primarily reflects the temperature at the emission level of infrared radiation, leading to the interpretation that isotopic depletion associated with convection is the result of lower condensation temperature. In cloudy conditions, this reflects the altitude of the cloud top. Therefore, in the tropics, lower (higher) OLR values also correspond to higher (lower) cloud top and echo top altitudes, average altitude of rainfall within clouds, and likely associated with cooler (warmer) temperatures at which precipitation forms in clouds [e.g., *Mechem and Oberthaler*, 2013, Figure 5]. Based on echo tops radar data, previous studies in Puerto Rico and Hawaii concluded that rain δ^{18}O seasonality is influenced by atmospheric temperatures (temperature effect [*Dansgaard*, 1964]) that correspond to different cloud heights associated with the seasonal climate patterns [*Scholl et al*., 2009; *Scholl and Coplen*, 2010]. Rainfall δ^{18}O depletion that occurs during summer corresponds to deep convection and high cloud height associated with low-pressure systems, while during winter orographic precipitation and high-pressure systems are predominant where rainfall δ^{18}O enrichment is controlled by the limited cloud height under the trade wind inversion (TWI) layer [*Scholl et al*., 2009]. In ice core studies, the relationship between ice δ^{18}O and temperatures at mean condensation levels has been proposed for the interpretation of the tropical ice core records [*Thompson et al*., 2000, 2003]. Modeling studies in the western U.S. have also revealed the relationship between rainfall isotope seasonality and condensation height in temperate latitudes [e.g., *Buenning et al*., 2012, 2013].

Research on rainfall stable isotopes in the Maritime Continent Indonesia region may provide an opportunity to evaluate processes that control modern precipitation. Seasonal rainfall isotopic variations in this region have been linked to local or regional precipitation amounts [*Kurita et al*., 2009], and moisture origins [*Suwarman et al*., 2013], and are influenced by the strength of regional convective activity [*Moerman et al*., 2013; *Kurita*, 2013]. In the southern part of the central mountain ranges of Papua, Indonesia (New Guinea; 4°S, 137°E), the annual movement of the ITCZ causes low (high) OLR values during austral summer (winter) from December to March (May to October). However, *Aldrian and Dwi Susanto* [2003] identified the rainfall seasonality in this region as antimonsoonal, marked by a distinct peak during austral winter and relatively low rainfall during austral summer. This condition provides this region with a unique climate regime as the precipitation amount and OLR values are positively correlated on seasonal timescales, in contrast to the typical relationship in the tropics. Therefore, it is a challenge to directly evaluate the influence of precipitation amount

and convective activity on the isotope ratios in tropical rainfall from this region. It is also important to investigate the influence of moisture dynamics and the impact of ENSO interannual variations on rainfall isotopic ratios in this region, as it is located in the heart of the West Pacific Warm Pool (WPWP). ENSO events can significantly alter the amplitude of seasonal rainfall in Papua [*Prentice and Hope*, 2007]. Papua usually experiences drier conditions during El Niño events [*Sukri et al*., 2003; *Permana*, 2011].

Here we present stable isotope analyses of 1332 rain samples collected daily during the period from January 2013 to February 2014 (ENSO-normal period) and December 2014 to September 2015 (El Niño period). The collection sites are located at various elevations along the southern slope of the central mountain ranges in Papua. The controls on daily to seasonal isotopic variations in precipitation are investigated with respect to local surface temperature, local/regional precipitation amount, and convective activity based on both in situ and satellite data. The influences of moisture dynamics on rainfall isotopic ratios are examined for moisture origins and transport history with air mass back trajectories and for moisture convergence. Furthermore, the influence of atmospheric temperature at mean condensation level on rainfall isotopic values is examined with respect to the altitude of latent heat (LH) release and cloud fraction in the troposphere. The isotopic ratios during ENSO-normal and El Niño periods are also investigated to provide insights into the key climate factors controlling isotopic variability in precipitation on interannual timescales in the region and, ultimately, inform our understanding of the information preserved in tropical ice cores from Papua glaciers.

2. Site Description and Climate

Papua (8°S–0°S, 130°E–141°E), which was known as Irian Jaya before 2002, is the largest and easternmost of the 34 provinces in the Republic of Indonesia. With a land area of 319,036 km^2 (16.62% of the Indonesian region), Papua and West Papua Provinces occupy the western half of New Guinea Island. Papua is bordered on the east by Papua New Guinea (PNG) and is surrounded by the Pacific Ocean to the north, the Arafura Sea (AS) to the south, and the Banda Sea (BS) to the west (Figure 1a). The island is divided from the east-southeast to the west-northwest by mountain ranges that exceed 3500 m above sea level (m asl), including the highest peak, Puncak Jaya (4884 m asl). The Papua landmass is covered mostly by tropical rainforest with wetlands in some coastal regions and grasslands in the high mountains.

The climate setting of Papua, which is located within the WPWP, is controlled mainly by the annual movement of the ITCZ [*McAlpine et al*., 1983; *Prentice and Hope*, 2007]. During austral summer (the "northwest season," December to March), the climate is dominated by the monsoon westerlies which result from veering of the northeast trade winds over the equator due to heating over the New Guinea landmasses (Figure 1b). The southeast trades flow over the entire Papua region during the austral winter (the "southeast season," May to October) (Figure 1c) [*Prentice and Hope*, 2007]. The temperature regime is typically equatorial with a seasonal range of ~1 to 3°C and a diurnal range of ~6 to 14°C. Moderately high temperatures occur at sea level, varying between 22°C and 34°C. The southern mountain ranges of Papua experience maximum (minimum) temperature in December–February (June–August), but the more equatorward regions experience two temperature maxima (minima) in May and November (February and July). The average regional surface lapse rate is ~5.0°C/km as determined by weather station data. Below 2500 m asl, the average level of the top of the atmospheric boundary layer [*Prentice and Hope*, 2007], the lapse rate is 5.2°C/km and above that altitude the rate decreases to 4.6°C/km [*Permana*, 2011].

Because of the surrounding oceans, Papua is one of the wettest regions on Earth with many sites receiving 2500–4500 mm of precipitation annually [*Prentice and Hope*, 2007]. Due to its location within the WPWP, there is little seasonal variability in rainfall. For most parts of Papua, rainfall maxima (minima) occur during the northwest (southeast) season, but in the southern part of the central mountain ranges the seasonality is reversed (see the study area in Figure 1) [*Aldrian and Dwi Susanto*, 2003]. The annual precipitation in this region ranges between ~5000 and 12,000 mm with the highest amount (~12,500 mm/yr) recorded at Mile50 station (4.28°S, 137.01°E; 617 m asl) [*Permana*, 2011]. During the northwest season all parts of the island are almost continuously wet (Figure 1b), with the monsoon westerlies prevailing up to about 600 mb. The weather pattern is dominated by a low-pressure system associated with enhanced deep convective activity which is driven by the position of the ITCZ in the Southern Hemisphere. During the southeast season the southern part of the island experiences drier conditions with minimum rainfall in June–July (Figure 1c). However, the rainfall amount in the lower part of the study area is higher than during the northwest season. In the southeast season, the trade wind

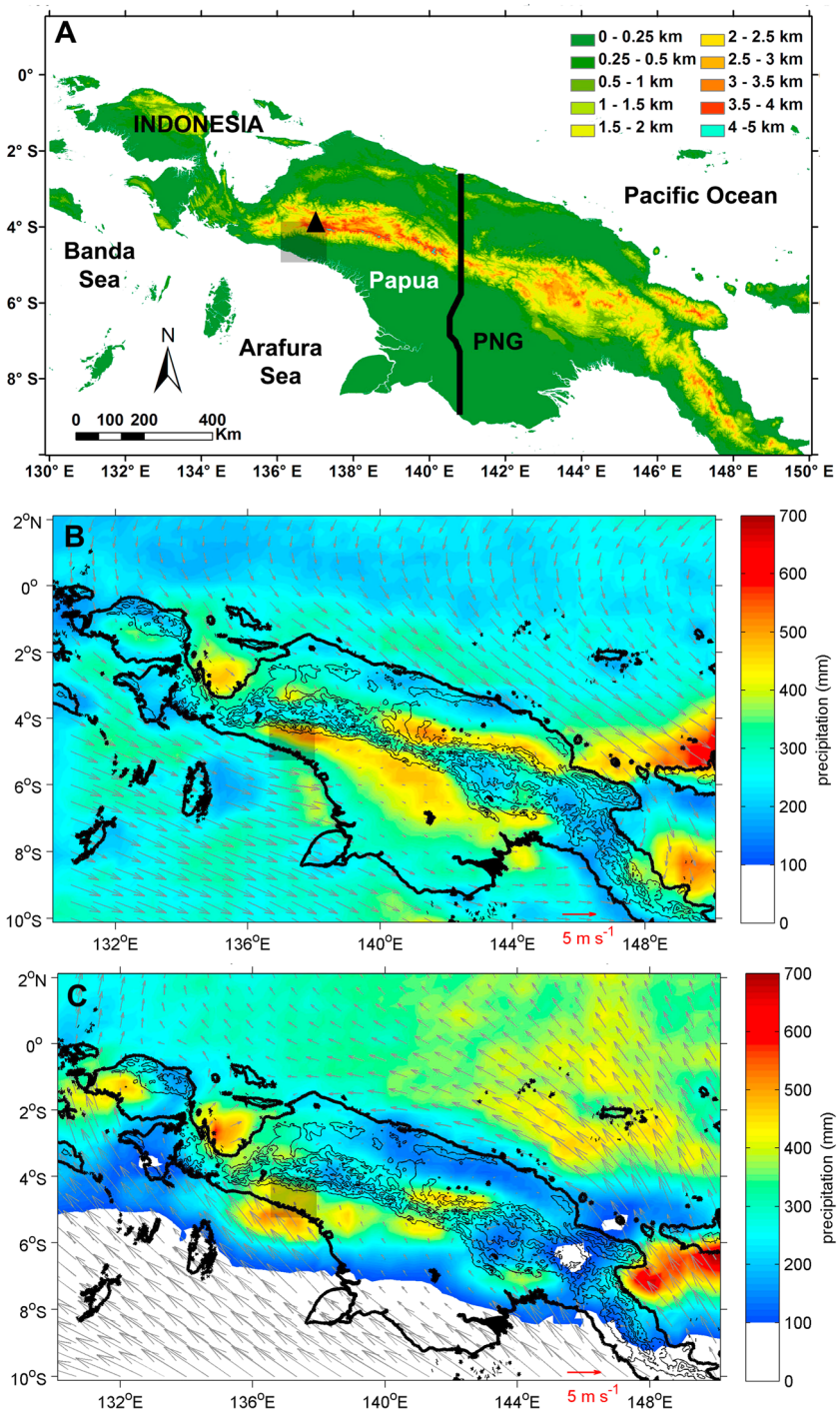

Figure 1. (a) Topography of Papua Province and its borders (NASA SRTM 90 m [*Jarvis et al.*, 2008]). The small black triangle marks the highest peak of Puncak Jaya. (b) Mean monthly precipitation (shaded, TRMM 3B43V7 products) and mean 10 m winds (vector, NASA MERRA reanalysis) from January 1998 to December 2013 for January. (c) As in Figure 1b but for July. The black shadow box (Figures 1a–1c) is the study area.

inversion (TWI) layer is present at about 2000 m asl south of the mountains in Papua as a result of the ITCZ position in the Northern Hemisphere [*McAlpine et al.*, 1983; *Prentice and Hope*, 2007]. The TWI layer, indicated by a strong temperature inversion, is a controlling factor for cloud development which caps local convective circulation and mixing processes. During this season, meteorological data from lowland stations demonstrate that rainfall at nighttime (6 P.M.–6 A.M. local time) is much higher than at daytime (6 A.M.–6 P.M. local time), with differences

Table 1. Number of Samples for Each Station by Month[a]

Month	PORT	TMK	KK	TPR	GRS	Total
Jan 2013	3	3	3	3	2	14
Feb 2013	15	18	24	18	18	93
Mar 2013	15	8	25	16	6	70
Apr 2013	20	9	28	25	0	82
May 2013	19	13	22	26	4	84
Jun 2013	24	7	25	24	2	82
Jul 2013	25	16	31	27	22	121
Aug 2013	11	6	24	27	11	79
Sep 2013	13	11	25	18	0	67
Oct 2013	13	0	30	17	0	60
Nov 2013	10	0	28	9	0	47
Dec 2013	16	0	29	20	0	65
Jan 2014	8	0	2	20	0	30
Feb 2014	0	0	0	5	0	5
Dec 2014	11			18	7	36
Jan 2015	18			25	18	61
Feb 2015	10			22	24	56
Mar 2015	11			20	16	47
Apr 2015	19			20	23	62
May 2015	16			15	3	34
Jun 2015	21			23	0	44
Jul 2015	14			13	10	37
Aug 2015	11			10	9	30
Sep 2015	10			16	0	26
Total	333	91	296	437	175	1332

[a]The empty row splits the two collection periods. See Text S1 for details.

of up to 250–350 mm/month occurring from June to August [*Permana*, 2011]. Conversely, highland stations receive at least as much rainfall during the day as at night.

This diurnal variation in the southeast season is mainly caused by local wind regimes and orographic lifting resulting in a shallow local convective system that is limited by the presence and the strength of TWI. During the day, particularly in late afternoon, the rainfall on the lowland is caused mainly by southeast trade winds transporting moisture from the Arafura Sea, enhanced by upslope anabatic (valley) winds and sea breezes at the southern coast. As it interacts with steep topography, orographic lifting of the moisture produces high rainfall over the slopes and highlands. At night, strong southeast trade winds converge with downslope katabatic (mountain) winds enhanced by land breezes at the southern coast, leading to offshore convergence and producing high nocturnal rainfall on the southern lowlands [*McAlpine et al*., 1983]. A similar nocturnal rainfall mechanism also occurs during the northwest season due to offshore convergence of katabatic flow with monsoon westerlies [*McAlpine et al*., 1983]. The only difference between the two seasons is the presence of the TWI, suggesting that more nocturnal rainfall originates from shallow convection systems during the winter. The impacts of trade winds and local wind circulation on the diurnal rainfall have been observed in Papua New Guinea [*McAlpine et al*., 1983] and the island of Hawaii [*Chen and Nash*, 1994; *Esteban and Chen*, 2008] which has analogous topography to southern Papua. The influence of topography on the diurnal precipitation cycle over New Guinea Island based on satellite products and modeling was discussed by *Zhou and Wang* [2006]. Furthermore, the diurnal cycle over the island of New Guinea during summer is systematically modulated by intraseasonal variability in large-scale circulation patterns such as the MJO [*Ichikawa and Yasunari*, 2008]. A recent study suggests that diurnal variation, rather than monsoon variation, is the dominant factor that controls precipitation intensity in the study area [*Christianto*, 2014].

3. Methods and Data

3.1. Sample Collection and Analysis

While a Papua ice core drilling project conducted on the glaciers near Puncak Jaya by the Byrd Polar and Climate Research Center (BPCRC) was underway in June 2010, 83 rain samples for stable isotope analysis were collected from different elevations daily over 2 weeks [*Permana*, 2011]. For this study, we used 1332 rain samples that were collected daily in two collection periods. The first period was from January 2013 to February 2014 at five stations, and the second was from December 2014 to September 2015 at three stations at altitudes ranging from 9 to 3945 m asl along a ~90 km transect across the southern mountain ranges (Table 1). The sampling sites were located near weather stations operated by PT Freeport Indonesia (PTFI) (Figure 2): Portsite (PORT; 4.83°S, 136.84°E; 9 m asl), Timika (TMK; 4.53°S, 136.89°E; 37 m asl), Kuala Kencana (KK; 4.41°S, 136.86°E; 67 m asl), Tembagapura (TPR; 4.14°S, 137.09°E; 1900 m asl), and Grasberg (GRS; 4.04°S, 137.12°E; 3945 m asl). In March 2008 the TPR weather station was moved to Mile 66 (M66; 4.15°S, 137.1°E; 2350 m asl); thus, due to their close proximity, rainfall isotopes from TPR were compared with meteorological data from M66. The climatology for each collection site is also shown in Figure 2.

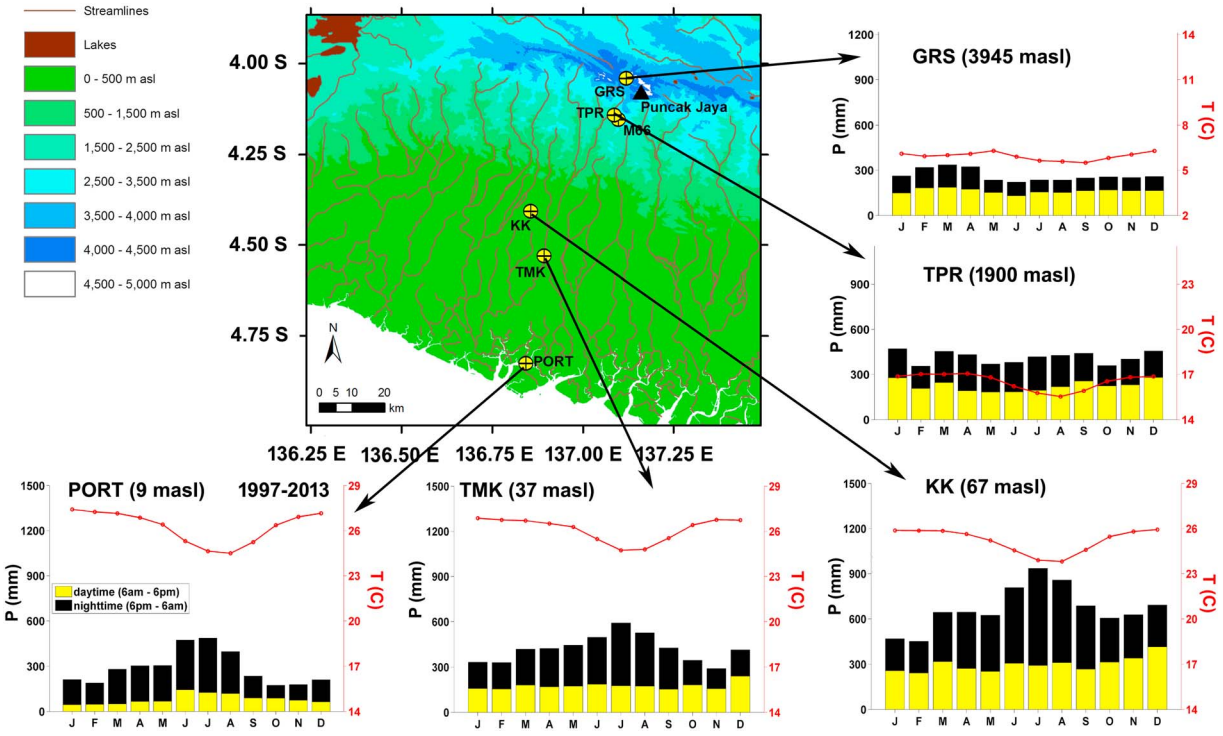

Figure 2. The rain collection sites and climatology. The climatology is based on observation data from 1997 to 2013, except for TPR which is from 1997 to 2007. Note that the temperature scale is different for GRS.

The details of the collection processes and a description of the rain collectors are located in Text S1 and Figure S1 in the supporting information, respectively. The first collection period for TMK, KK, and TPR began on 29 January 2013, while at PORT it began earlier (26 January 2013) and at GRS it began later (30 January 2013). The fewest number of samples were collected at the highland station GRS from May to June 2013 due to a tunnel collapse at the PTFI training facility in mid-May. The second collection period, at PORT and TPR, started on 11 December 2014, while at GRS it started on 13 December 2014.

Rainfall isotopic ratios of oxygen ($\delta^{18}O$) and hydrogen (δD) were measured at the BPCRC stable isotope laboratory using a cavity ring-down spectrometer (Picarro L2120-i water isotope analyzer). A well-known global relationship between average $\delta^{18}O$ and δD in natural waters has been defined by *Craig* [1961] as the global meteoric water line (GMWL) and derived by the equation $\delta D = 8{*}\delta^{18}O + 10$. In any particular region, this relationship is defined as the local meteoric water line (LMWL). *Dansgaard* [1964] defined the *y* axis intercept value of the MWL as the deuterium excess ($d = \delta D - 8{*}\delta^{18}O$). The reported estimates of uncertainty attributed to rainfall $\delta^{18}O$ and δD measurements are ±0.2‰ and ±1.5‰, respectively. An uncertainty of ±1.5‰ for *d* excess values is calculated from the quadratic combination of the uncertainties of $\delta^{18}O$ and δD.

3.2. Climate Data

Local meteorological data during the collection period, including local precipitation amounts and surface temperature, were obtained from PTFI weather stations and the local office of the Agency for Meteorology Climatology and Geophysics of Indonesia (BMKG) in Timika. Daily regional precipitation and monthly latent heating data were derived from the National Aeronautics and Space Administration (NASA)-Tropical Rainfall Measuring Mission (TRMM) satellite products 3B42 V7 (0.25°×0.25° grid) and 3A12 V7 (0.5°×0.5° grid), respectively. Unfortunately, the TRMM 3A12 products are only available up to March 2015 as the instruments on TRMM were turned off on 8 April 2015. Regional convective activity data were obtained from the National Oceanic and Atmospheric Administration (NOAA) interpolated OLR data set on a 2.5°×2.5° grid [*Liebmann and Smith*, 1996]. OLR data at higher resolution were derived from the NASA-Modern-Era Retrospective Analysis for Research and Application (MERRA) reanalysis as a variable of upward longwave flux at top of atmosphere from 1979 to present with a resolution of 0.67° longitude and 0.5° latitude [*Bosilovich*, 2008;

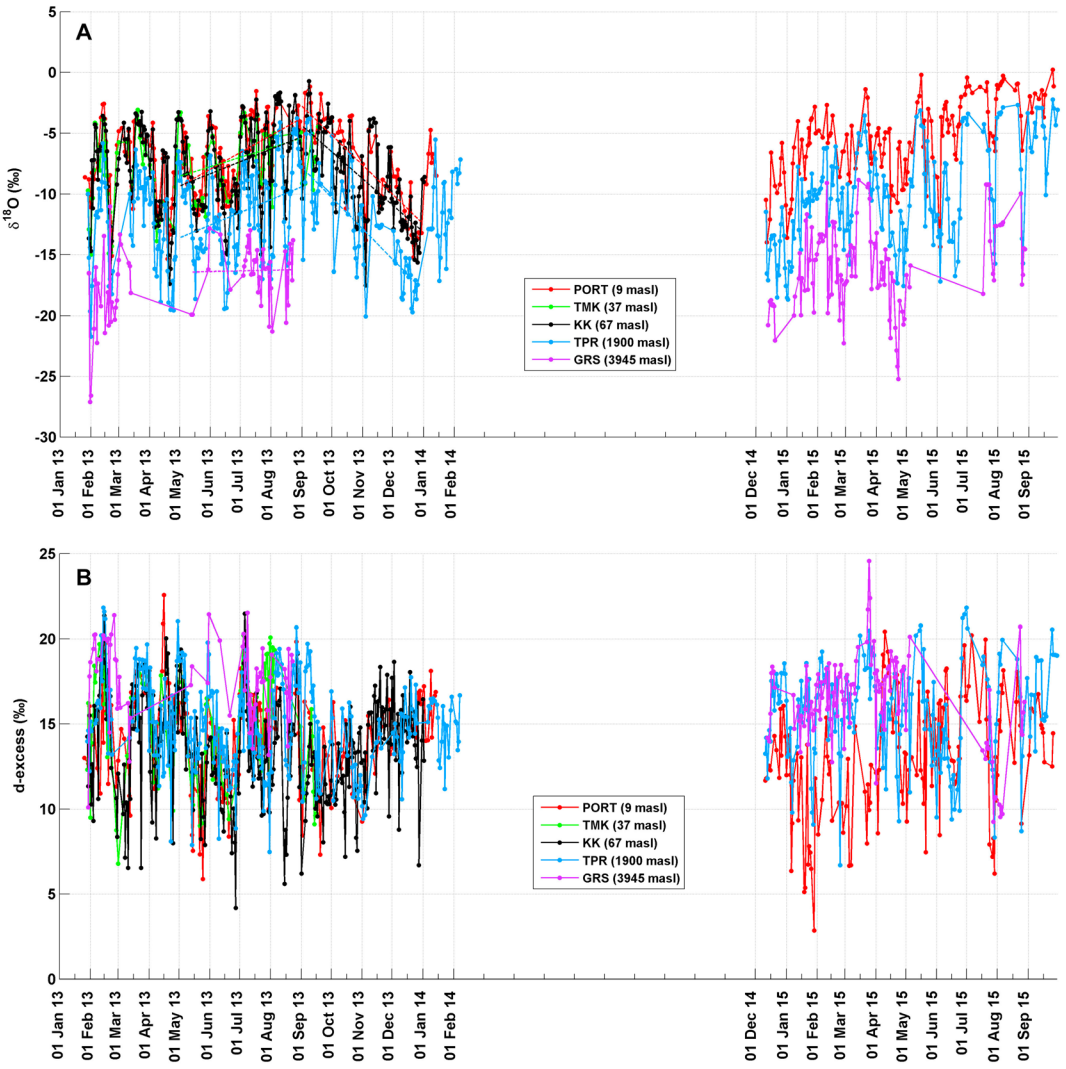

Figure 3. (a) Time series of daily rainfall $\delta^{18}O$ for all stations with dashed lines representing the linear trend over particular time intervals. (b) Time series of daily *d* values for all stations.

NASA, 2011; *Rienecker et al*., 2011]. Since the NOAA OLR data are only available up to 31 December 2013, MERRA OLR data were used in this study demonstrating that they compare well during the period of 2013 (Figure S2). The moisture origins and moisture transport paths were identified and simulated using the Hybrid Single-Particle Lagrangian Integrated Trajectory (HYSPLIT) back trajectory model [*Draxler and Rolph*, 2014] combined with National Centers for Environmental Prediction (NCEP) reanalysis data at 12 h time steps back to 5 days at 1000 m above ground level (m agl). The calculated back trajectories were also conducted at different elevations using Global Data Assimilation System for testing sensitivity. In addition, surface wind and cloud fraction data were obtained from MERRA reanalysis. Sea surface temperatures (SSTs) were provided by the NOAA Extended Reconstructed Sea Surface Temperature version 3b data set [*Smith et al*., 2008].

4. Results

4.1. Stable Isotope Variations ($\delta^{18}O$, δD, and *d*)

Daily rainfall $\delta^{18}O$ and deuterium excess ($d = \delta D - 8*\delta^{18}O$) data from all stations are shown in Figure 3 (δD data are shown in Figure S3). Detailed statistics of daily rainfall $\delta^{18}O$, δD, and *d* are described in Table 2. The results show that the more depleted $\delta^{18}O$ values occur with increasing elevation, which demonstrates the nature of the altitude effect. The calculated regional isotopic lapse rate for $\delta^{18}O$ is −2.4‰/km and for

Table 2. Descriptive Statistics of Daily Rainfall $\delta^{18}O$, δD, and d Values for All Stations

	Jan 2013 to Feb 2014 (ENSO-Normal Year)					Dec 2014 to Sep 2015 (El Niño Year)					All Samples	
Station	Minimum	Mean	Amount Weighted	Maximum	Range	Minimum	Mean	Amount Weighted	Maximum	Range	Mean	Amount Weighted
						$\delta^{18}O$ (‰)						
PORT (9 m asl)	-15.35	-7.32	-6.78	-1.18	14.16	-14.34	-5.38	-6.23	0.21	14.55	-6.50	-6.57
TMK (37 m asl)	-14.99	-7.89	-7.84	-3.06	11.93						-7.89	-7.84
KK (67 m asl)	-17.50	-8.11	-8.28	-0.71	16.79						-8.11	-8.28
TPR (1900 m asl)	-21.72	-12.07	-12.02	-3.76	17.96	-18.66	-10.11	-10.96	-2.21	16.45	-11.26	-11.64
GRS (3945 m asl)	-27.10	-17.09	-17.72	-11.02	16.08	-25.22	-15.94	-16.12	-8.83	16.39	-16.37	-16.87
						δD (‰)						
PORT (9 m asl)	-107.30	-44.33	-39.93	6.20	113.50	-106.22	-29.98	-36.46	14.63	120.85	-38.25	-38.58
TMK (37 m asl)	-110.43	-48.56	-47.09	-6.20	104.23						-48.56	-47.09
KK (67 m asl)	-126.72	-51.45	-52.92	6.22	132.94						-51.45	-52.92
TPR (1900 m asl)	-158.62	-81.66	-81.19	-9.44	149.18	-136.23	-65.24	-72.31	2.84	139.07	-74.84	-78.00
GRS (3945 m asl)	-199.02	-119.15	-124.34	-73.68	125.34	-186.23	-111.28	-112.13	-51.11	135.12	-114.20	-117.84
						d (‰)						
PORT (9 m asl)	5.88	14.24	14.30	22.57	16.69	2.84	13.03	13.37	20.42	17.58	13.73	13.94
TMK (37 m asl)	6.78	14.52	15.62	20.21	13.43						14.52	15.62
KK (67 m asl)	4.17	13.43	13.35	21.46	17.29						13.43	13.35
TPR (1900 m asl)	7.48	14.92	14.94	21.82	14.34	6.69	15.65	15.40	21.82	15.13	15.22	15.10
GRS (3945 m asl)	10.10	17.57	17.39	21.51	11.41	9.25	16.28	16.85	24.56	15.31	16.76	17.10

δD is −18.2‰/km. These values are comparable to the calculated isotopic lapse rates of −2.3‰/km for $\delta^{18}O$ and −18.0‰/km for δD during the ~2 week collection period in June 2010 [*Permana*, 2011], as well as with the global isotopic lapse rate of approximately −2.8‰/km for $\delta^{18}O$ [*Poage and Chamberlain*, 2001]. This altitude effect is equivalent to a temperature effect of 0.48‰/°C for $\delta^{18}O$ and 3.64‰/°C for δD, based on the surface lapse rate of 5.0°C/km [*Permana*, 2011]. In general, all stations show a similar temporal variation of daily rainfall $\delta^{18}O$, which suggests that a common regional factor controls the temporal isotopic variability in the region.

The mean weighted d values range from 13.35‰ at KK to 17.10‰ at GRS (Table 2), which demonstrate an increase of d value with elevation at a rate of 0.68‰/km. Increasing d values with elevation have also been reported in the tropical montane rainforest of the Amazon Basin [e.g., *Windhorst et al.*, 2013]. The d values tend to increase with elevation at high relative humidity [*Gonfiantini et al.*, 2001], which is prevalent in the Papua region. The mean d value of all samples is ~15‰, which is greater than the GMWL intercept of 10‰ [*Craig*, 1961]. The possible cause of the high d value in this region is a land surface recycling through the surrounding tropical rainforests during transport to the collection sites [*Salati et al.*, 1979; *Windhorst et al.*, 2013]. As with $\delta^{18}O$, the daily d variations at all stations show similar patterns suggesting relatively similar moisture sources and transport pathways into the region (Figure 3b).

In the first collection period (ENSO-normal year), the most enriched $\delta^{18}O$ (δD) of −0.71‰ (6.22‰) was recorded at KK, while the most depleted $\delta^{18}O$ (δD) of −27.10‰ (−199.02‰) was recorded at GRS (Table 2). The mean weighted $\delta^{18}O$ ranges from −6.78‰ at the lowest elevation (PORT) to −17.72‰ at the highest elevation (GRS), while the weighted δD ranges from −39.93‰ to −124.34‰ at these same stations. The ranges of $\delta^{18}O$ and δD among all the stations are 11.93‰ to 17.96‰ and 104.23‰ to 149.18‰, respectively. There are no linear trends on daily rainfall $\delta^{18}O$ at the four lowest stations between February and April 2013, while linear trends increase from May to August 2013, decrease from September to December 2013, and increase from January to February 2014 (Figure 3a). Due to lack of data at GRS, daily rainfall $\delta^{18}O$ variations could initially only be surmised to follow the patterns seen at the other stations. It was only after the second collection period that the GRS trends could be confirmed. On the other hand, the daily d values on seasonal timescales demonstrate little linear trend (Figure 3b).

In the second collection period (El Niño year), the amount-weighted stable isotope signatures ($\delta^{18}O$ and δD) in rain samples are more enriched than during the first period (ENSO-normal) at all stations (Table 2). The d values are lower than during the ENSO-normal period, but the differences are insignificant because they fall within the ±1.5‰ range of uncertainty. In addition, the ranges of $\delta^{18}O$ and δD values are similar between El Niño and the ENSO-normal periods.

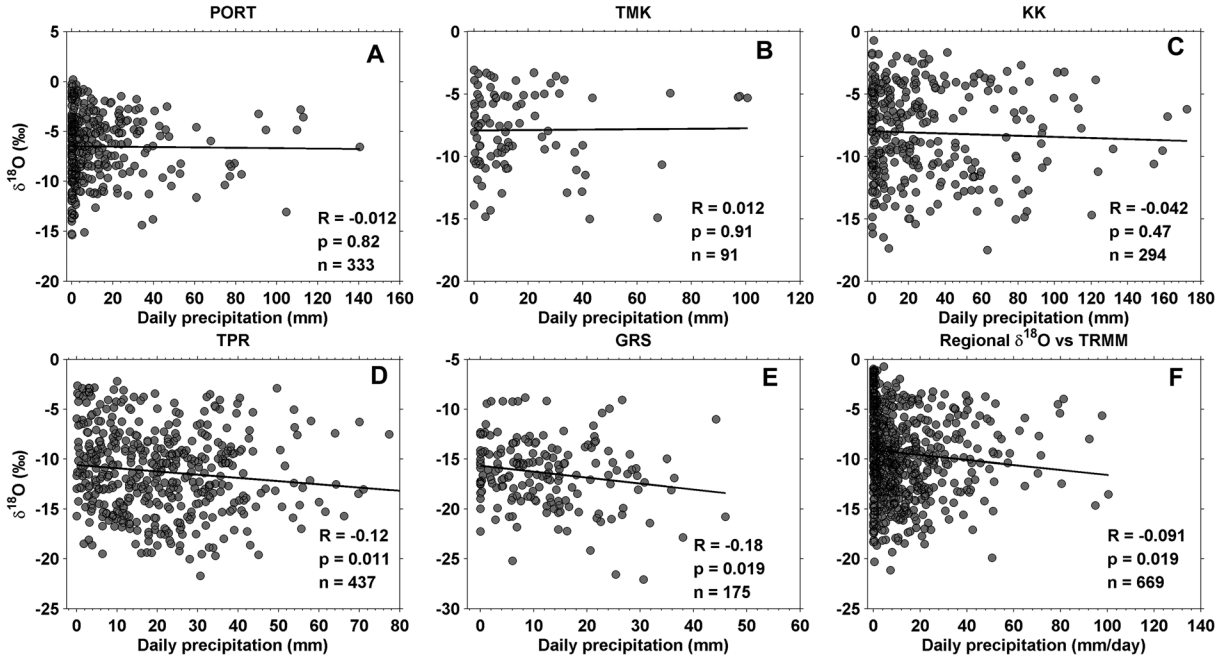

Figure 4. Relationships between daily rainfall $\delta^{18}O$ and daily local precipitation amount at (a) PORT, (b) TMK, (c) KK, (d) TPR, and (e) GRS. (f) The relationship between daily rainfall $\delta^{18}O$ composite and daily regional precipitation (mean precipitation from TRMM at 4.375–4.875°S, 136.875°E). Regression lines are in black.

4.2. Local Meteoric Water Lines (LMWLs)

The slopes of the LMWLs range between 7.90 and 8.54 (Figure S4) and are comparable to the GMWL slope of 8. However, the intercept values (*d*) range between 14.27‰ and 19.04‰ and are higher than the GMWL value of 10. By considering samples from all stations, the regional MWL (RMWL) is calculated as $\delta D = 7.98\ \delta^{18}O + 14.38$ ($n = 1332$, $R^2 = 0.99$).

Considering all samples from lowland (PORT), midland (TPR), and highland (GRS) stations, there are no significant changes in the MWL observed during the El Niño period ($\delta D = 7.94\ \delta^{18}O + 14.38$; $n = 433$, $R^2 = 0.99$) compared to the ENSO-normal period ($\delta D = 7.99\ \delta^{18}O + 14.86$; $n = 512$, $R^2 = 0.99$).

5. Discussion

5.1. Daily Variability of Rainfall $\delta^{18}O$

Due to similar daily isotopic variations among the stations, all daily rainfall $\delta^{18}O$ are amount weighted, composited, and then linearly interpolated to obtain the daily regional rainfall $\delta^{18}O$ (Figure S5). Based on statistical analyses, there are no significant correlations between daily rainfall $\delta^{18}O$ and daily local precipitation amounts at the three low-elevation stations (Figures 4a–4c), while at middle- and high-elevation stations, the correlations are significantly negative but significantly weak (Figures 4d and 4e). At a regional scale, no correlation exists between the daily rainfall $\delta^{18}O$ and daily precipitation amounts (mean precipitation from TRMM at 4.375–4.875°S and 136.875°E) ($R = -0.091$, $p = 0.02$; Figure 4f). This suggests that the local/regional precipitation amount does not exert a major control over isotopic ratios in the area on a daily basis.

On the other hand, the correlation coefficients between daily rainfall $\delta^{18}O$ and daily local surface temperature at all stations are significantly negative but weak (Figures 5a–5e). These inverse relationships suggest that local surface temperature is also not the main driver of rainfall $\delta^{18}O$ in the region. Instead, a statistically significant but weak positive relationship ($R = 0.46$, $p < 0.001$; Figure 5f) is observed between daily regional rainfall $\delta^{18}O$ and daily regional convective activity (mean OLR values from MERRA at 4.5–5°S, 136.67°E), signifying that convective activity is likely the main control of rainfall $\delta^{18}O$ in the region.

The positive correlation between daily regional rainfall $\delta^{18}O$ and OLR values increases from 0.22 ($p < 0.01$) during the ENSO-normal period to 0.61 ($p < 0.01$) during the El Niño period. Meanwhile, the negative correlation

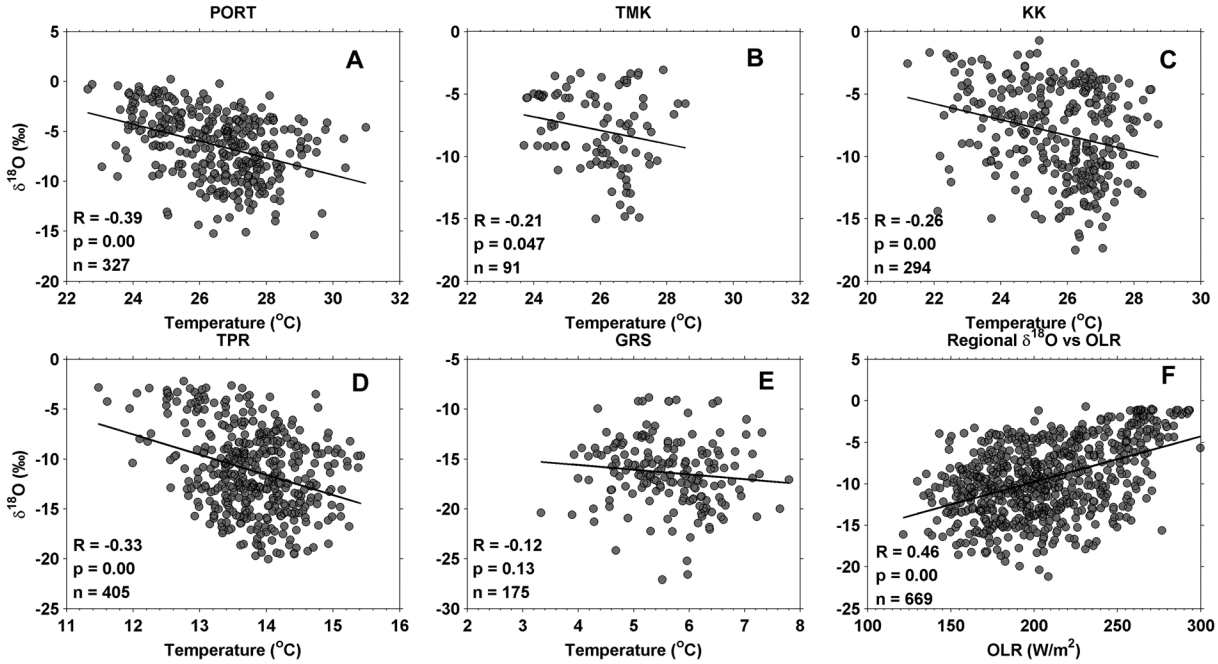

Figure 5. (a–e) As in Figure 4 but with daily local surface temperature. (f) The relationship between $\delta^{18}O$ and daily regional convective activity (mean OLR values from MERRA at 4.5–5.0°S, 136.67°E).

between daily regional rainfall $\delta^{18}O$ and regional precipitation amount is significant during the El Niño period ($R = -0.25$; $p < 0.01$), but not during the ENSO-normal period ($R = 0.08$; $p = 0.13$). This negative relationship is likely due to much drier conditions throughout Papua during El Niño events, particularly in austral winter [*Sukri et al*., 2003; *Prentice and Hope*, 2007].

In order to investigate the relationship between $\delta^{18}O$ and climate variables on longer timescales, Figures 6a and 6b show the correlations between running means of daily $\delta^{18}O$ and local/regional precipitation and OLR during the two collection periods. With increased daily averaging, correlations between the regional rainfall $\delta^{18}O$ and OLR values become even stronger during the two collection periods, suggesting an even greater role for regional convective activity on rainfall $\delta^{18}O$ at longer timescales. In contrast, negative correlations between rainfall $\delta^{18}O$ and local/regional precipitation amount are stronger only during the El Niño event, whereas during the ENSO-normal period, no significant correlations exist up to 10 day running means. Interestingly, the correlations are significantly positive but weak at greater than 10 day running means with a range of 0.11 (at 10 day running means) to 0.35 (at 60 day running means). Furthermore, correlations between rainfall $\delta^{18}O$ and local precipitation remain positive at lowland and negative at highland stations during the ENSO-normal period.

In addition, convective processes may have integrated impacts on rainfall $\delta^{18}O$ over several previous days. The integration effect of convective activity has been observed in other monsoon regions [*Risi et al*., 2008a; *Vimeux et al*., 2011; *Tremoy et al*., 2012; *Moerman et al*., 2013; *Gao et al*., 2013]. In order to assess the influence of the temporal integration of precipitation and convective activity, Figures 6c and 6d show the correlations between daily local/regional $\delta^{18}O$ and running means of OLR and precipitation amount during the two collection periods. Daily regional rainfall $\delta^{18}O$ has a stronger positive correlation with OLR averaged over the previous 5–7 days ($R = 0.43$, $p < 0.01$ in the first period and $R = 0.78$, $p < 0.01$ in second period). Meanwhile, the negative correlations are more significant between daily rainfall $\delta^{18}O$ and mean regional precipitation over the previous 5–9 days ($R = -0.18$, $p < 0.01$ in the first period and $R = -0.52$, $p < 0.01$ in the second period). The most significant negative correlations between daily local rainfall $\delta^{18}O$ and running means of local precipitation at most stations occur over the previous 3 to 15 days averaging in both collection periods. These analyses agree with the time-integrative nature of rainfall $\delta^{18}O$ and support the hypothesis of the weeklong "memory" of rainfall $\delta^{18}O$ which may reflect the approximately weeklong atmospheric residence time of water vapor in the region [*Moerman et al*., 2013].

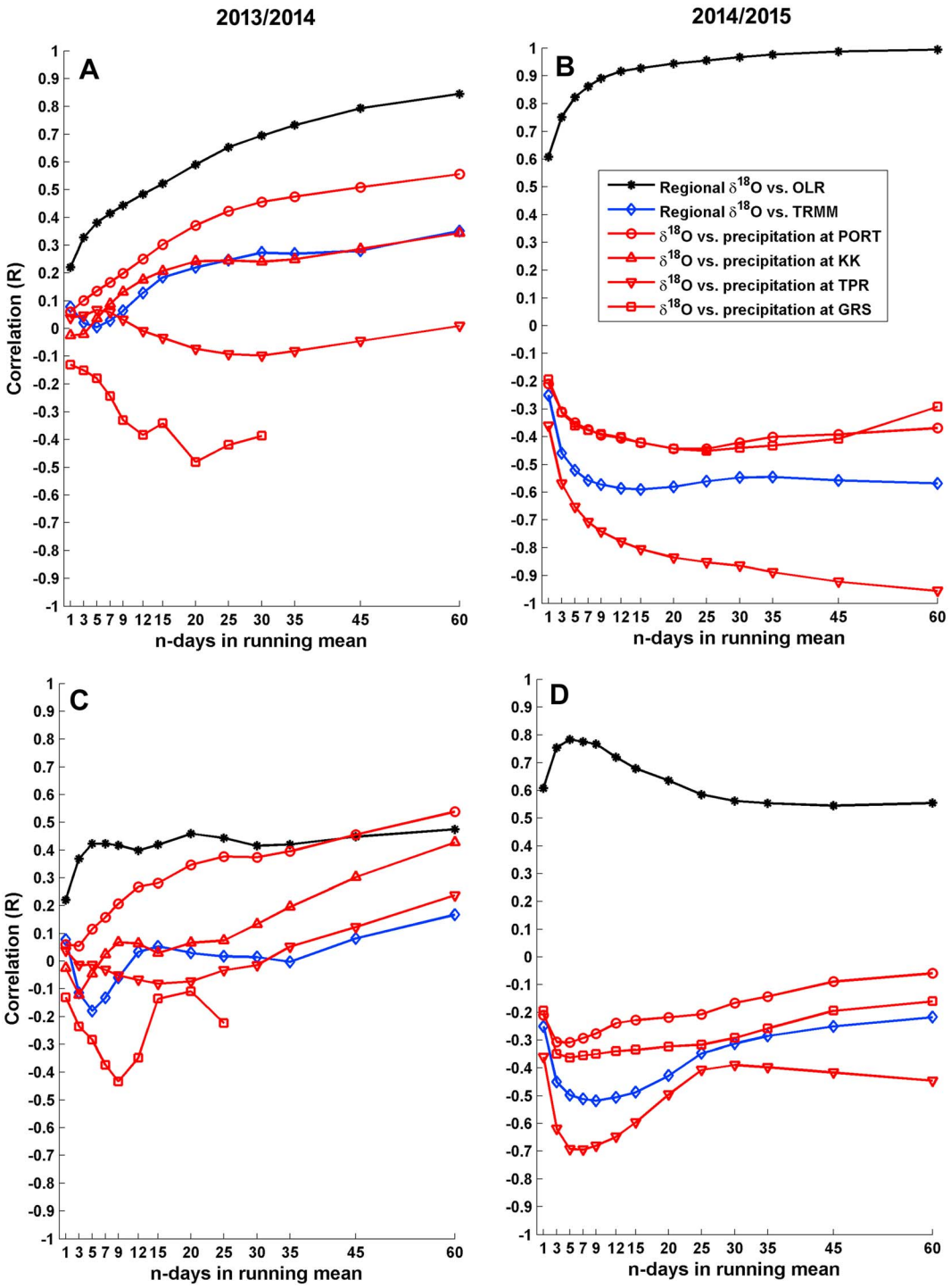

Figure 6. (a) Correlations between "*n*"-day running means of daily rainfall $\delta^{18}O$ and daily climate variables for the first collection period. (b) Correlations between daily rainfall $\delta^{18}O$ and *n*-previous day averages of climate variables for the first collection period. (c) As in Figure 6a and (d) as in Figure 6b but for the second collection period. Climate variables include local precipitation, regional precipitation (TRMM derived), and regional convective activity (OLR).

The integrative convection property of $\delta^{18}O$ has been explained by the progressive isotopic depletion of local water vapor by downdraft recycling process in the convective system. Furthermore, the shorter memory effect during the rainy season has been related to the more intensive and frequent convective activity in the region [*Vimeux et al*., 2011].

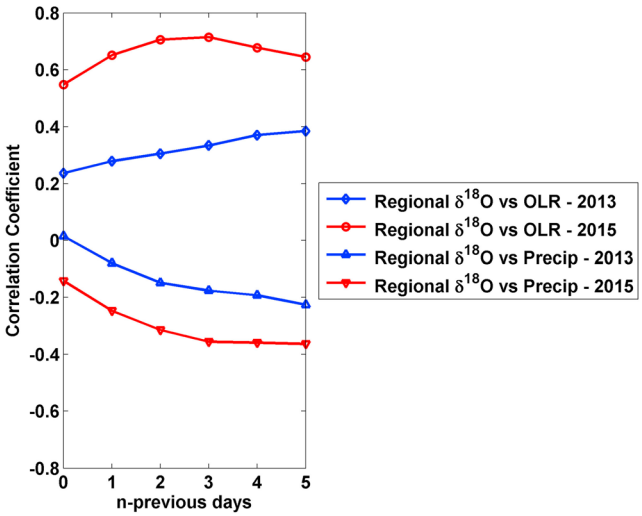

Figure 7. Correlation coefficients between daily regional rainfall $\delta^{18}O$ and mean OLR (MERRA) and cumulative precipitation (TRMM) along the back trajectories over *n*-previous days at 1000 m agl in 2013 and 2015.

The spatial integrative effects of convective activity and precipitation on rainfall $\delta^{18}O$ variation are also examined based on air mass trajectories. Daily air mass back trajectories during 2013 and 2015 were calculated using the Hybrid Single-Particle Lagrangian Integrated Trajectory (HYSPLIT) back trajectory model [*Draxler and Rolph*, 2014] combined with NCEP reanalysis data at 12 h time steps back to five previous days at 1000 m above ground level (m agl). The correlation coefficients between daily regional rainfall $\delta^{18}O$ and daily average OLR (MERRA), as well as with the cumulative regional precipitation (TRMM) along the back trajectories, are shown for 2013 and 2015 in Figure 7. Both parameters have significant effects on rainfall $\delta^{18}O$ variation, with convective activity more significantly correlated than precipitation amount. These correlations are not significantly changed by using different source of meteorology data nor by using different starting elevations in the HYSPLIT model (Figure S6).

The correlation coefficients over the five previous days are comparable to the temporal integrative effect of convective activity and precipitation on rainfall $\delta^{18}O$ (Figures 6c and 6d), suggesting a significant spatiotemporal integrated effect of convective activity and precipitation in the region. Although the correlation between daily rainfall $\delta^{18}O$ and precipitation is improved when precipitation amounts are cumulated along the back trajectories from the upwind region, it is still weaker than the spatially integrated effect of convective activity on rainfall $\delta^{18}O$, indicating that convective activity is more important than precipitation amount on controlling rainfall $\delta^{18}O$. This is consistent with previous studies [*Gao et al.*, 2013; *Samuels-Crow et al.*, 2014; *Lekshmy et al.*, 2014] which indicate that the upwind regional convective activity is a good controlling factor on rainfall $\delta^{18}O$ variation in the tropics.

Consistently positive relationships between rainfall $\delta^{18}O$ and OLR on daily and longer timescales during ENSO-normal and El Niño conditions indicate that regional convective activity explains a larger portion of rainfall $\delta^{18}O$ variability. Furthermore, the spatiotemporal integrative convection over 5–7 days seems to be the strongest control in the region. In contrast, inconsistent temporal relationships between local/regional precipitation amount and rainfall $\delta^{18}O$ indicate that precipitation amount is not a major control on rainfall $\delta^{18}O$ variability.

5.2. Intraseasonal Variability of Rainfall $\delta^{18}O$

Previous studies [*Risi et al.*, 2008a; *Vimeux et al.*, 2011; *Tremoy et al.*, 2012; *Gao et al.*, 2013; *Moerman et al.*, 2013] have demonstrated correlations between tropical rainfall $\delta^{18}O$ and large-scale convective activity at intraseasonal timescales. *Kurita et al.* [2011] showed that rainfall isotopic variation in Maritime Continent Indonesia is associated with the MJO intraseasonal cycle. The MJO cycle is defined as the eastward propagation of mesoscale convective systems (MCSs) with period of ~30–90 days which is characterized by the deep organized convective systems and cloud clusters along the tropical band causing high precipitation [*Madden and Julian*, 1972]. The regional rainfall $\delta^{18}O$ is more significantly positively correlated with the OLR values over increasing time averages (Figures 6a and 6b). The regional rainfall $\delta^{18}O$ time series is characterized by peak-trough variations with average amplitude of ~5‰ and with a periodicity of ~20–60 days using a band-pass filter (Figure S7). Using spectral analyses, regional rainfall $\delta^{18}O$ and OLR time series also indicate similar periodicities of ~15–70 days during the two collection periods which resemble the MJO periodicity in the region (Figures 8a and 8b). This is consistent with the findings of *Moerman et al.* [2013] in northern Borneo (4°N, 114°E), northwest of Papua. In their study, the authors concluded that the MJO strongly influences the intraseasonal variability of rainfall $\delta^{18}O$, with major depletion events ($\delta^{18}O$ shifts up to ~10‰) coinciding with the active (wet) phases of the MJO.

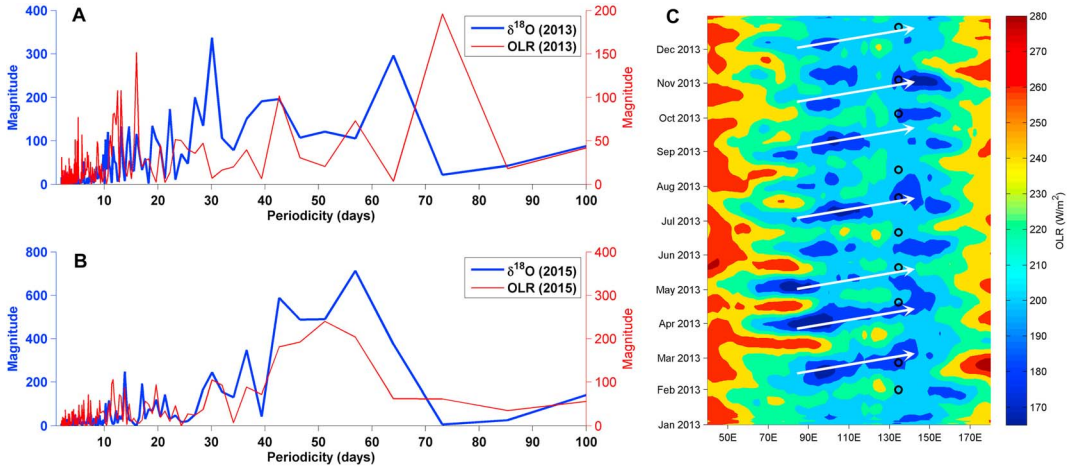

Figure 8. (a) Periodicity of rainfall $\delta^{18}O$ and OLR time series in 2013 using spectral analyses. (b) As in Figure 8a but for 2015. (c) Time-longitude diagram of daily NOAA interpolated OLR filtered with a 25–100 days band-pass (Lanczos) filter and averaged over 0–5°S for the period of 1 January to 31 December 2013. Open black circles indicate the timing of rainfall $\delta^{18}O$ composite depletion events that occur during the time windows. White arrows illustrate the eastward propagation of enhanced convective activity associated with the active phases of the MJO intraseasonal cycle.

As Papua is also located within the MJO influenced area, major $\delta^{18}O$ depletion events in this region are also likely associated with the active phases of the MJO. Figure 8c shows that major regional $\delta^{18}O$ depletion events mostly coincide with enhanced regional convective activity (low OLR values) during its eastward propagation in the tropical region.

5.3. Seasonal Variability of Rainfall $\delta^{18}O$

The seasonal amount-weighted $\delta^{18}O$ values during the two collection periods at most stations are generally marked by austral summer depletion and austral winter to spring enrichment; however, enrichment is also observed in March (Figures 9a–9e). The seasonal correlations between monthly $\delta^{18}O$ and local precipitation amount vary among the stations; they are significantly negative at TPR ($R = -0.76$, $p = 0.004$), but insignificantly negative at GRS ($R = -0.29$, $p = 0.44$), while the relationship is insignificantly positive at TMK ($R = 0.51$, $p = 0.16$) and KK ($R = 0.46$, $p = 0.14$) and there is no correlation at PORT ($R = -0.02$, $p = 0.95$). On the other hand, the correlations with surface temperatures are negative and significant at PORT ($R = -0.65$, $p = 0.02$), KK ($R = -0.59$, $p = 0.04$), and TPR ($R = -0.60$, $p = 0.04$) but insignificant at TMK ($R = -0.57$, $p = 0.11$) and GRS ($R = -0.51$, $p = 0.16$). Regionally, the seasonal variation of the monthly regional amount-weighted $\delta^{18}O$ resembles the seasonal variation of regional convective activity with a significantly positive correlation ($R = 0.80$, $p = 0.002$; Figure 9f). Moreover, an insignificant negative relationship is observed between monthly regional amount-weighted $\delta^{18}O$ and TRMM regional precipitation on seasonal timescales ($R = -0.30$, $p = 0.35$; Figure 9f). These results suggest that regional convective activity plays a more important role than local/regional precipitation amount in controlling rainfall $\delta^{18}O$ on seasonal timescales.

The annual movement of the ITCZ is the main driver of seasonal convective activity in the tropics. Its position in the austral summer (monsoon) season causes low-pressure systems which lead to enhanced deep convective systems and organized MCSs with deep cumulonimbus clouds generating high precipitation. During the austral winter, a high-pressure system in the southern slope of central Papua supports the isolated shallow convection and formation of shallow cumulus clouds due to local wind circulation and topography which also generates high precipitation, particularly at lower elevations. The results of this study are consistent with previous studies that suggest that local/regional precipitation amount is not the main control on seasonal rainfall $\delta^{18}O$ variation but rather depends on large-scale convective activity [*Kurita*, 2013; *Lekshmy et al.*, 2014]. For instance, total rainfall at KK in July and August 2013 (winter) was 1533 mm and 1360 mm, respectively, with monthly weighted $\delta^{18}O$ of −6.5‰ and −5.0‰, respectively, and associated OLR values of 220 W m^{-2} and 225 W m^{-2}, respectively. Meanwhile, in February and December (summer) 2013 total rainfall was 593 mm and 575 mm, respectively, with monthly weighted $\delta^{18}O$ of −8.0‰ and −12.2‰, respectively, and associated OLR values of 182 W m^{-2} and 186 W m^{-2}, respectively. Similar patterns are also observed regionally using TRMM precipitation data.

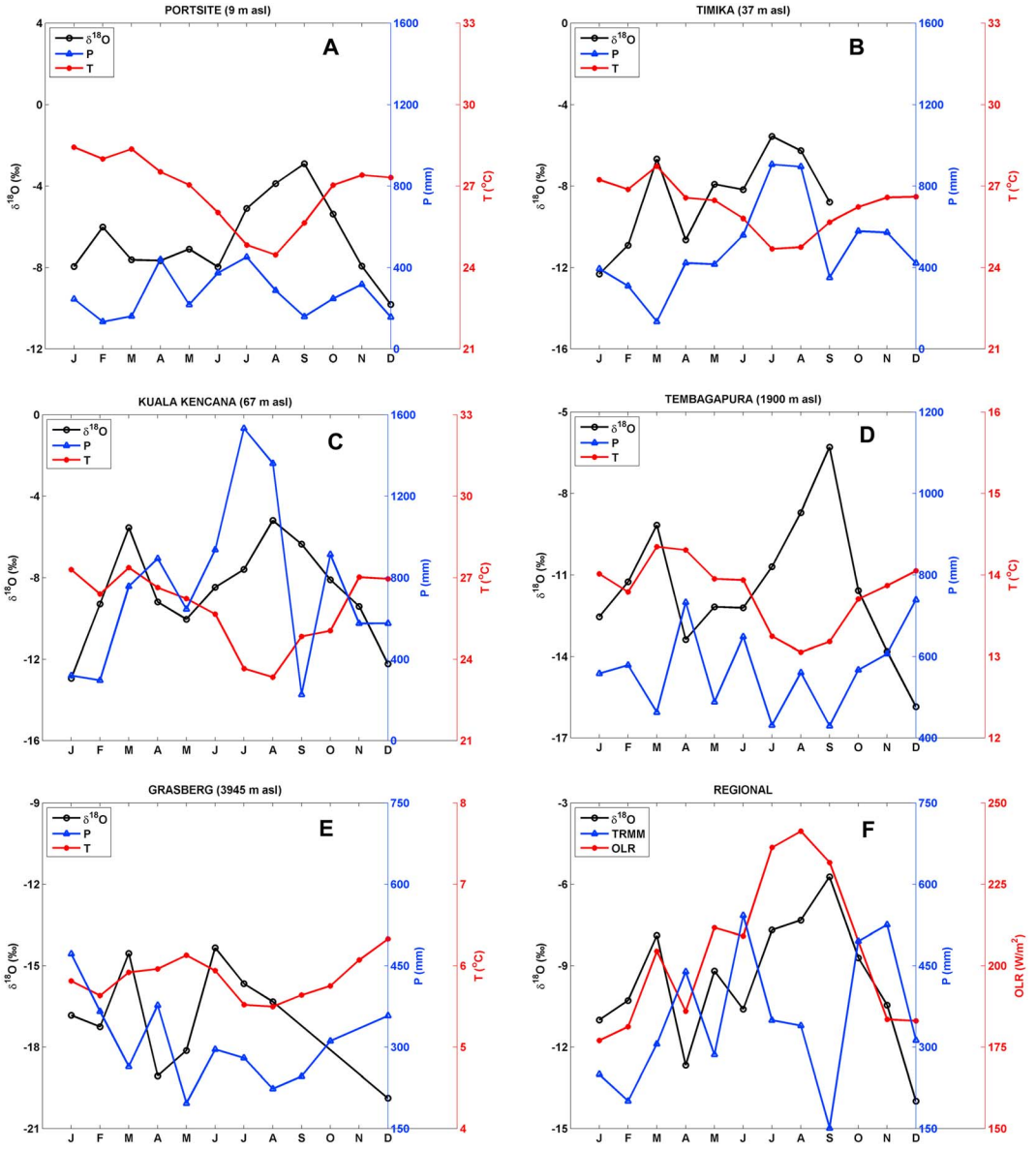

Figure 9. Seasonal amount-weighted $\delta^{18}O$, precipitation amount, and temperature at (a) PORT, (b) TMK, (c) KK, (d) TPR, and (e) GRS stations. (f) Seasonal regional amount-weighted $\delta^{18}O$, regional convective activity (OLR), and regional precipitation (TRMM) during the two collection periods.

Large amounts of heavy rainfall during winter 2013 at KK and other lowland stations are likely not generated by deep enhanced convection from higher and colder clouds associated with low-pressure system but are more possibly produced by shallow convection due to local wind circulation and topography setting, with the convection being capped by the TWI layer, which is associated with high-pressure systems.

In addition, local comparisons among three stations (PORT, KK, and TPR) in 2013 that lie within a range of ~80 km (Figure 2) indicate that mean annual rainfall $\delta^{18}O$ is not influenced by the annual precipitation amount but likely by the altitude effect associated with temperature changes. For instances, PORT and KK are lowland stations (altitudes of 9 and 67 m asl, respectively) that had similar average annual rainfall $\delta^{18}O$ in 2013 (-6.8 and -8.3‰, respectively) but are very different in the total annual precipitation (~4000 and ~9600 mm, respectively). On the other hand, KK and TPR (1900 m asl) had similar annual precipitation amounts in 2013 (~9600 and ~9000 mm, respectively) but differ in the mean annual rainfall $\delta^{18}O$ (-8.3 and -12‰, respectively) which is likely due to the altitude difference (Figure S8).

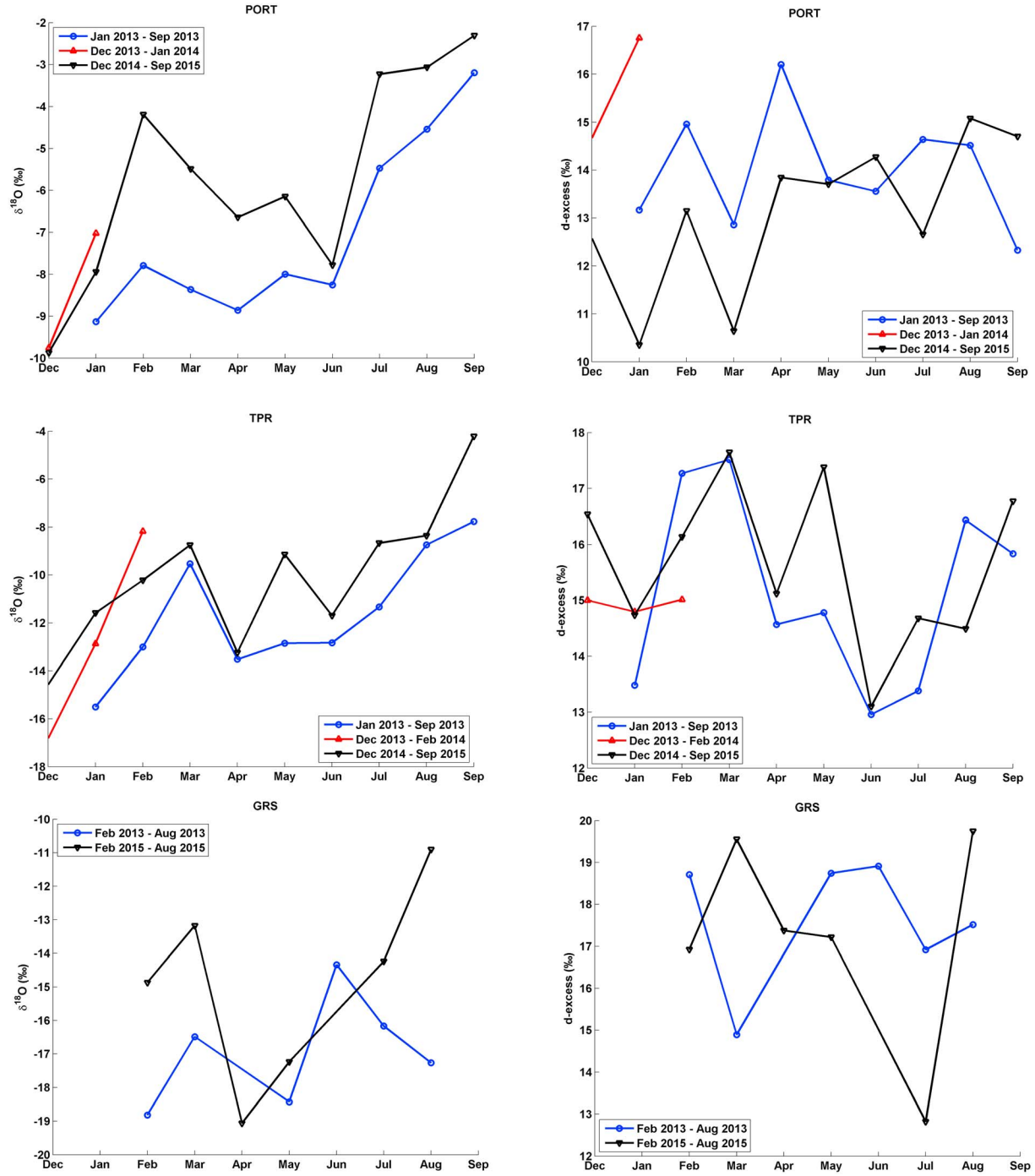

Figure 10. Comparison of monthly amount-weighted rainfall $\delta^{18}O$ and *d* values between ENSO-normal period (January 2013 to February 2014) and El Niño period (December 2014 to September 2015) at PORT (December to September), TPR (December to September), and GRS (February to August) stations.

5.4. Comparison of Rainfall Isotopic Composition Between ENSO-Normal and El Niño Periods

The comparison of mean monthly amount-weighted isotopic values between the ENSO-normal period (2013/2014) and the El Niño period (2014/2015) shows that the $\delta^{18}O$ (δD) has increased by ~1.6‰ (~11.4‰) at PORT in the El Niño period from December to September. At TPR, $\delta^{18}O$ (δD) has also increased by ~1.8‰ (~14.8‰) from December to September, while at GRS, $\delta^{18}O$ (δD) has increased by ~2‰ (~15‰) from February to August (Figure 10; δD data are not shown). In contrast, the *d* value has decreased by ~1.2‰ at PORT in the El Niño period with a decrease of ~2.6‰ during austral summer

(December to April), whereas the *d* values at TPR and GRS are relatively constant with differences of 0.6‰ and −0.6‰, respectively (Figure 10).

On the other hand, meteorological data comparison between 2013 and 2015 suggests that temperatures at lowland (PORT) and midland (TPR) stations are relatively cooler during El Niño than during the ENSO-normal period which is likely due to the cooler SSTs in the western Pacific (Figure S9). Meanwhile, at high altitude (GRS), temperature is cooler in summer but warmer in winter during El Niño than during the ENSO-normal period. A warmer winter in the Papua highland is possibly due to heat circulation in the tropical troposphere which warms the tropospheric temperatures, usually for up to 6 months, after El Niño begins [*Sobel et al*., 2002]. As a result, local/regional precipitation at all elevations was lower during the El Niño than during the ENSO-normal period, with much drier conditions occurring during the winter (Figure S9). At the same time, the convective activity over Papua was suppressed during El Niño, as shown by higher OLR values in 2015 than in 2013 (Figure S9). This is likely the main cause for the observed enrichment of isotopic ratios in rainfall at all stations (Figure 10).

A decrease in *d* values during the El Niño period in the lowland station (Figure 10), particularly during summer, may be due to cooler SSTs around Papua as the warm pool shifts to the central Pacific. This leads to a decrease in evaporation rates and associated kinetic fractionation in the ocean and thus to decreased *d* values of evaporated water vapor and precipitation [*Merlivat and Jouzel*, 1979].

Over the ~2 year collection period that covered the ENSO-normal and the El Niño period, the correlation between δ^{18}O and local precipitation is negative and insignificant at PORT ($R = -0.14$, $p = 0.53$) but significant at TPR ($R = -0.56$, $p = 0.005$) and GRS ($R = -0.53$, $p = 0.04$). On the other hand, the δ^{18}O values are significantly negatively correlated with temperature at PORT ($R = -0.67$, $p < 0.001$) and TPR ($R = -0.61$, $p = 0.002$) but insignificant at GRS ($R = -0.33$, $p = 0.22$). At regional scales, a significant and negative correlation exists between δ^{18}O and precipitation ($R = -0.40$, $p = 0.05$) but a stronger significant positive correlation exists between δ^{18}O and OLR values ($R = 0.74$, $p < 0.001$) (Figure 11). Again, this suggests that regional convection, rather than precipitation, plays a dominant role in rainfall δ^{18}O variation during these periods.

5.5. Moisture Origins and Transport Pathways

On seasonal timescales, moisture origins and transport paths have been shown to influence isotopic ratios in precipitation by determining the initial stable isotopic ratios of water vapor and additional moisture evaporated from the land surface (land surface recycling) during transport, respectively [*Kurita et al*., 2009; *Breitenbach et al*., 2010; *Crawford et al*., 2013; *Suwarman et al*., 2013]. Initial isotopic compositions (δ^{18}O and *d* values) of evaporating water vapor can be affected by the SSTs and surface level relative humidity and wind speed at the site of evaporation [*Dansgaard*, 1964; *Clark and Fritz*, 1997; *Merlivat and Jouzel*, 1979].

For simplicity, it is assumed that back trajectories that were conducted in section 5.1 provide information about the moisture origin and transport paths. During January to March 2013 and December 2013 (austral summer), moisture originating from the seas to the northwest of Papua is transported to the collection sites by the monsoon westerlies (Figure 12a). Water vapor is moved across the Banda Sea, the Arafura Sea, and the northern Papua tropical rainforest before reaching the collection sites. In contrast, from May to October 2013 (austral winter) the southeast trade winds transported moisture from the seas to the southeast of Papua across the southern Papua tropical rainforest (Figure 12b). The moisture sources in April and November 2013 (transitional) are composed of a combination of both the seas to the northwest and southeast of Papua (not shown). Air mass trajectories in 2015 show a similar result as in 2013 (not shown).

During austral winter, water vapor originates from the seas to the southeast of Papua, which have long-term mean SSTs of 25–29°C, mean surface relative humidity of 72–82%, and mean surface wind speed of ~7 m/s (the southeast trade winds). These conditions are comparable to conditions during the summer over the seas to the northwest of Papua where the initial water vapor originates, with long-term mean SSTs of 27–29°C, mean surface relative humidity of 74–84%, and mean surface wind speed decreases from ~7 m/s to ~3–5 m/s as the northeast trade winds turn into the monsoon westerlies (Figure S10). The nearly identical meteorological conditions over the oceanic origins during both seasons in the Papua region may indicate that the isotopic compositions of evaporating water vapor are also nearly identical. A previous study conducted in Australia discusses the moisture sources to the south of Papua and suggests that there was no significant difference in the rainfall δ^{18}O when the majority of the moisture originated from oceanic sources [*Crawford et al*., 2013].

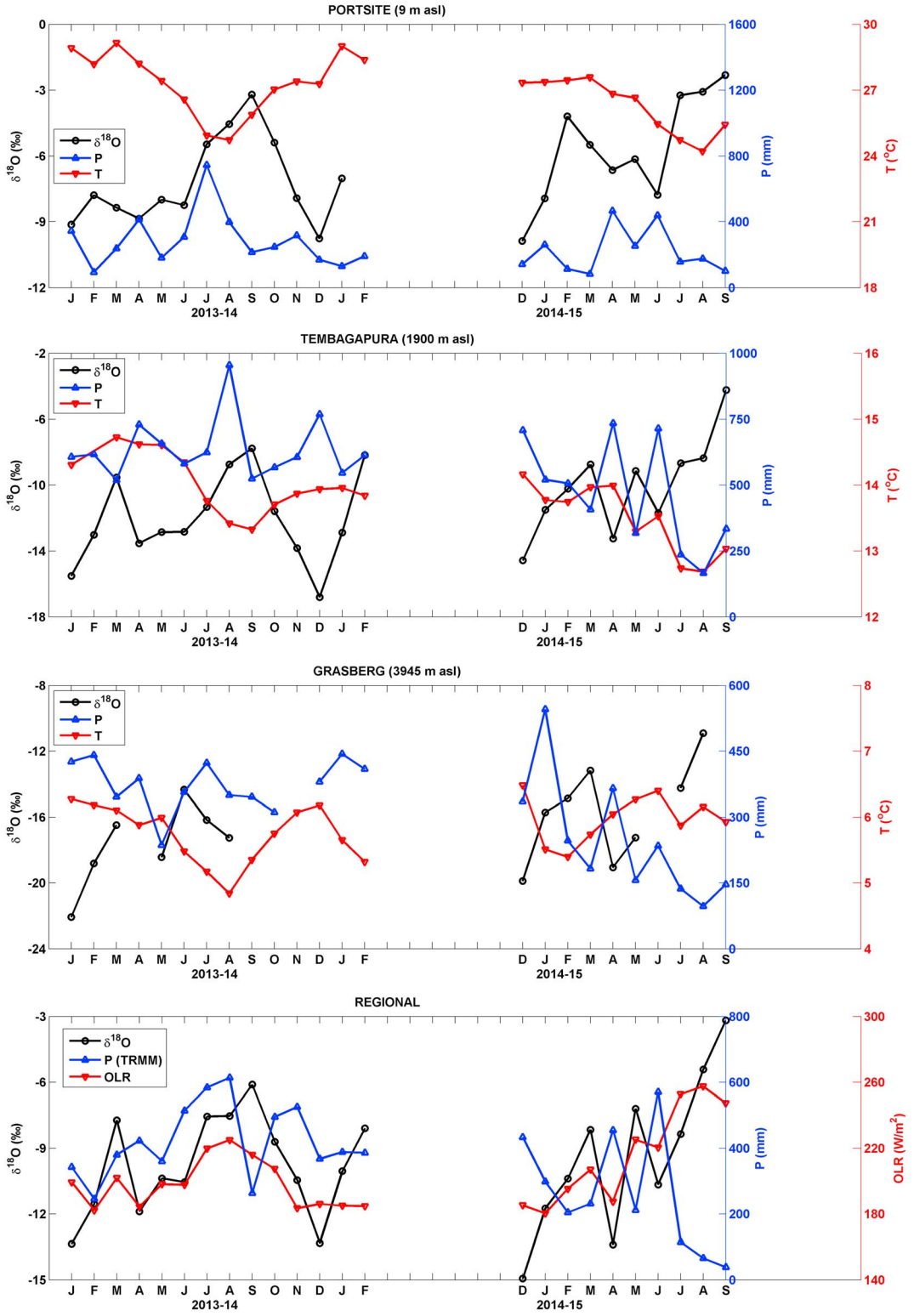

Figure 11. Time series comparison of monthly amount-weighted $\delta^{18}O$, temperature, precipitation, and OLR values over the two collection periods at local and regional scales.

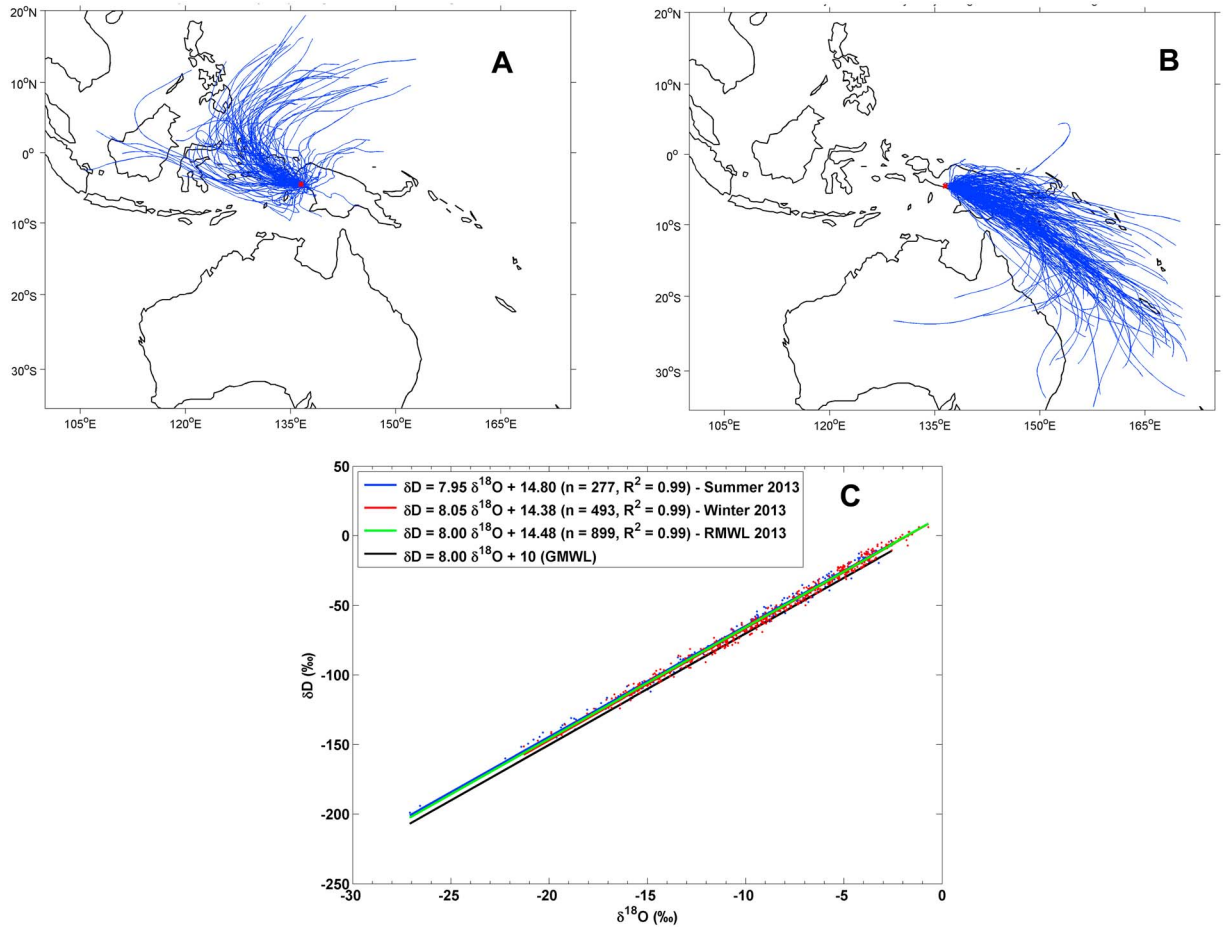

Figure 12. (a) Air mass back trajectories over five previous days at 1000 m agl simulated by HYSPLIT model combined with NCEP reanalysis data over the study area for summer (December–March) 2013. (b) As in Figure 12a but for winter (May–October) 2013. (c) Regional meteoric water lines (RMWLs) for summer and winter during the first collection period. Summer covers the period January–March 2013 and December 2013 to February 2014, while winter covers the period May–October 2013.

The additional moisture from land surface recycling during transport from oceanic sources to the precipitation sites can have considerable impact on isotopic composition in precipitation [*Salati et al*., 1979]. The land surface recycling has been shown to yield precipitation with higher *d* values over the Amazon Basin [*Gat and Matsui*, 1991; *Windhorst et al*., 2013]. Additional recycled moisture within the air masses over the Amazon Basin also contributes to ^{18}O-enriched rainfall during austral winter when the southeast trade wind-related precipitation prevails [*Windhorst et al*., 2013]. In our study area, the mean *d* values at each station are higher than 10‰ during both the first and second collection periods (Table 2), suggesting the large contribution of recycled moisture to precipitation. During summer, additional evaporated moisture likely originates from terrestrial evaporation over the northern tropical rainforest, while during winter the recycled moisture comes from evaporation over the southern tropical rainforest. To evaluate the contribution of land surface recycling on seasonal rainfall δ^{18}O, the seasonal MWLs for summer and winter 2013 (ENSO-normal period) were calculated to derive the mean *d* values for each season. The result shows that the MWLs for summer and winter 2013 are very close, with intercept (*d*) values of 14.80‰ and 14.38‰, respectively (Figure 12c). The nearly equal *d* values suggest similarly significant contribution of land surface recycling in rainfall ^{18}O enrichment in both seasons. Consequently, land surface recycling only causes a minor seasonal effect on rainfall δ^{18}O in our study area (Figure 12c).

In addition, moisture convergence has been shown to affect the isotopic signature of tropical rainfall. *Moore et al*. [2014] suggest that a parameter *E*/*P* (*E* is surface evaporation, and *P* is precipitation), which represents the relative contribution of the converged vapor in precipitation, has a positive correlation with δD of precipitation. However, there is no significant correlation ($R = -0.04$, $p = 0.90$) between monthly regional rainfall

δD and E/P derived from MERRA reanalysis data in the study area during 2013 (Figure S11). This result indicates that moisture convergence also has no significant effect on seasonal rainfall $\delta^{18}O$ in the region.

Another factor that may affect the rainfall isotopic composition is a postcondensational effect such as raindrop (secondary) evaporation at the subcloud base during rainfall due to surface low humidity, which can decrease *d* values [*Rozanski et al*., 1993] and result in ^{18}O-enriched rainfall. However, this condition is unlikely to occur in a humid region such as Papua. This is supported by the observed mean relative humidity (generally above 80%) at all stations and elevations during 2013 (Figure S11). In summary, moisture origins and land surface recycling along the transport pathways contribute to a minor seasonal effect on rainfall isotopic composition in the region. Other factors such as moisture convergence and raindrop (secondary) evaporation during rainfall also have no significant influences on rainfall isotopic composition on seasonal timescales.

5.6. The Condensation Temperature Controls on Rainfall $\delta^{18}O$ Depletion Associated With Convective Activity

Although there are no significant correlations between local/regional precipitation or surface temperature and rainfall $\delta^{18}O$ on seasonal timescales, there is a significant positive correlation between OLR and rainfall $\delta^{18}O$, indicating that convective activity plays an important role on seasonal rainfall $\delta^{18}O$. Previous studies have reported this correlation to be related to the characteristics of stratiform/convective rainfall types associated with MCSs [*Kurita et al*., 2011; *Kurita*, 2013], but we propose to explore this relationship as the in-cloud temperature effects. In the tropics, the lower (higher) OLR values may reflect the higher (lower) cloud top and echo top altitudes of storm systems, with precipitation forming at cooler (warmer) temperatures in clouds [e.g., *Mechem and Oberthaler*, 2013, Figure 5]. Hence, positive correlations between rainfall $\delta^{18}O$ and OLR values can also be interpreted with respect to the temperature effect at the mean condensation level.

Instead of rainfall amount, rain condensation mechanisms that correspond to prevailing weather patterns and in-cloud properties when precipitation forms may have greater influence on rainfall isotopic composition. These effects have been suggested by previous studies in Costa Rica [e.g., *Rhodes et al*., 2006], in Maui, Hawaii [e.g., *Scholl et al*., 2007], in Puerto Rico [e.g., *Scholl et al*., 2009], in Ecuador [e.g., *Windhorst et al*., 2013], and in Sydney, Australia [e.g., *Crawford et al*., 2013]. In general, these studies concluded that more isotopically depleted precipitation originates in low-pressure systems associated with tropical storms and large-scale deep convection during the summer (monsoon) season. Conversely, the isotopically enriched precipitation originates in high-pressure systems associated with trade wind showers and/or orographic rainfall during the winter (dry) season. The seasonal weather patterns and rainfall $\delta^{18}O$ on the southern slope of Papua are consistent with those conditions, suggesting that the rain condensation mechanisms are important in controlling rainfall $\delta^{18}O$. By considering the minor effect of moisture sources, land surface recycling along the transport paths, moisture convergence, and raindrop (secondary) evaporation on seasonal rainfall $\delta^{18}O$, the relationship between rainfall $\delta^{18}O$ and convective activity on seasonal timescales is interpreted as a temperature effect at the mean condensation level.

It is difficult to empirically demonstrate this temperature effect [e.g., *Scholl et al*., 2009] without the echo top data from our study area. Fortunately, the mean echo top altitudes also correspond to the mean condensation levels which can be estimated by the latent heat (LH) release in the troposphere [e.g., *Thompson et al*., 2000]. The latent heat in the troposphere is released mainly by the condensation process when precipitation forms in clouds. The latent heating data sets have been retrieved by several different algorithms from TRMM satellite measurements [*Tao et al*., 2006]. For simplicity, the monthly LH vertical profile derived from TRMM product 3A12 V7 is used as a proxy of mean condensation level in the troposphere. Unfortunately, the LH products are available only over the ocean. Since our sites are close to the Arafura Sea, we use the closest gridded LH data at 136.25°E, 5.25°S to represent our sites in the current study. The vertical profile of monthly LH release from January 2013 to March 2015 is shown in Figure 13a. Generally, it exhibits two peaks in the troposphere, at ~0.5–2.5 km and at ~3–8 km. This is consistent with the double-peak structure of latent heating in the tropics suggested by previous studies [*Zhang et al*., 2010; *Liu et al*., 2015]. The shallow mode of the LH peak is associated with shallow convection systems that generate warm rain and low-level heating from shallow cumulus clouds (echo top less than 5 km) and partially from cumulus congestus clouds (echo top between 5 and 8 km). The deep mode of the LH peak corresponds to large, deep, organized MCSs with echo tops greater than 10 km [*Zhang et al*., 2010; *Liu et al*., 2015]. The deep mode of LH dominated the shallow mode during the northwest (monsoon) season in 2013 (except in March), while the dominant mode was reversed during the southeast

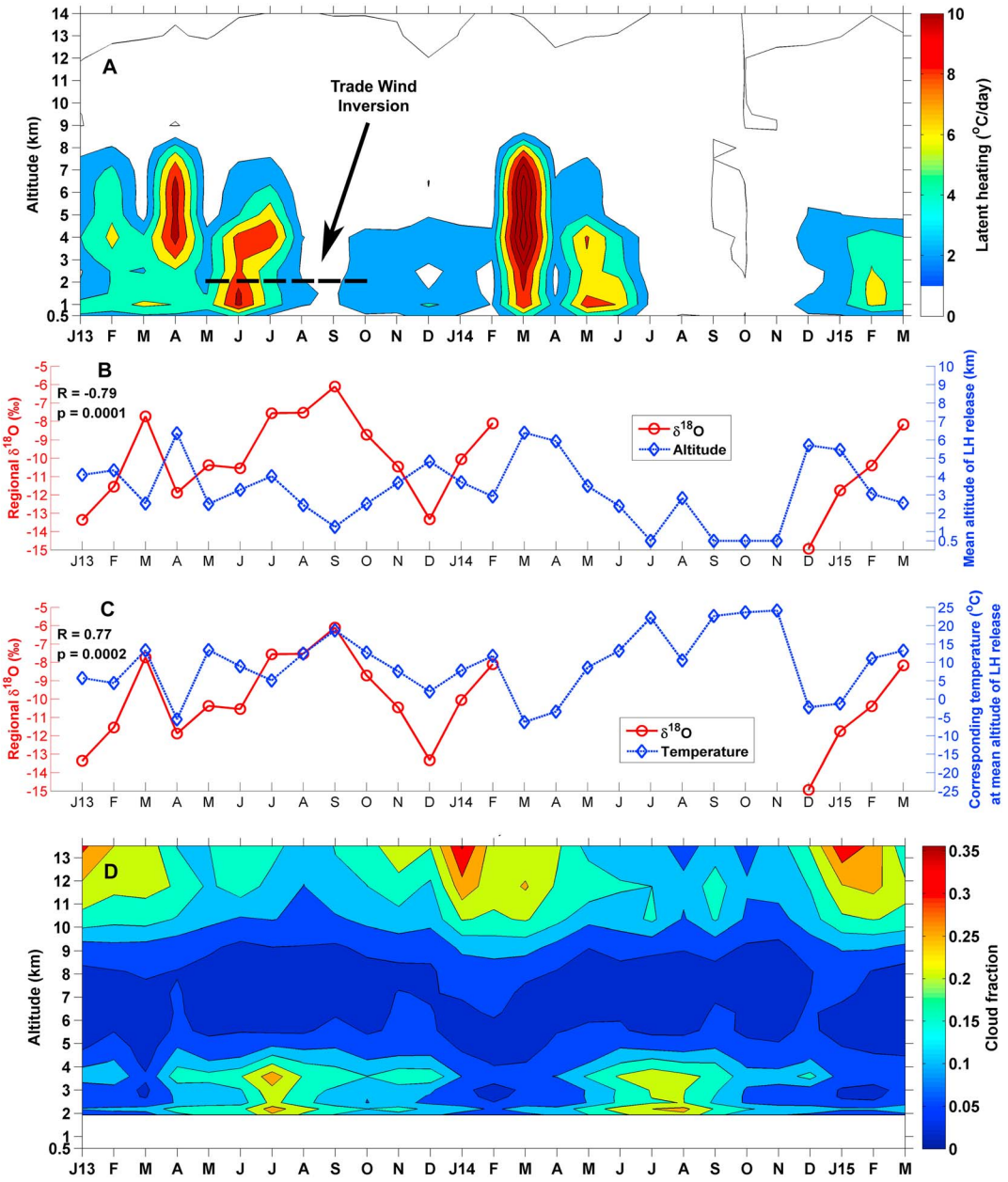

Figure 13. (a) The vertical profile of latent heat release at 136.25°E, 5.25°S from January 2013 to March 2015. (b) The relationship between monthly regional $\delta^{18}O$ and the mean altitude of latent heat release and (c) its corresponding atmospheric temperature. (d) The vertical profile of large-scale cloud fraction over the collection sites at 136.875°E, 4.375°S.

season (except in July). During September 2013 the troposphere was mainly dominated by the shallow mode of LH. In this study, we define the maximum altitude of LH release as the highest altitude with a heating rate of more than 1.6°C/d, which represents the average maximum latent heating per rainfall rate of 1 cm/d during the onset of the Indian monsoon and generates relatively high precipitation [*Magagi and Barros*, 2004]. In addition, the mean altitude of LH release is defined as the average altitude weighted by LH release below the maximum altitude. The corresponding temperature at the mean altitude of LH release may indicate the temperature at mean condensation level at which precipitation forms. An estimate of the atmospheric temperatures associated with the altitude of LH release was calculated based on the monthly temperature lapse rates and mean surface temperatures derived from PTFI meteorological data (Figure S12). The strong relationship between monthly regional $\delta^{18}O$ and the mean altitude of LH release ($R = -0.79$, $p = 0.0001$; Figure 13b) and

its corresponding atmospheric temperatures ($R = 0.77$, $p = 0.0002$; Figure 13c) from January 2013 to March 2015 compares well with the relationship between regional $\delta^{18}O$ and regional convective activity (OLR; $R = 0.68$, $p = 0.002$) over the same period. This result confirms that the effect of convection on rainfall $\delta^{18}O$ is associated with the temperature effect at the mean condensation level on seasonal rainfall $\delta^{18}O$.

The results of this study are consistent with previous studies in Puerto Rico [*Scholl et al.*, 2009] and in Hawaii [*Scholl and Coplen*, 2010], which suggest that the seasonal isotopic composition of tropical rainfall is correlated with cloud height and its corresponding (atmospheric) temperature. One common feature that exists among these oceanic islands (Puerto Rico, Hawaii, and our study area) is the appearance of the TWI layer during the winter season which effectively caps vertical motion from below and limits the height of cloud development. The prominent shallow mode of LH during winter 2013 evinces the TWI layer in our study area (Figure 13a). In this season, local convection and the interaction between strong southeast trade winds and diurnal winds result in intense precipitation which is mostly nocturnal below the TWI layer (Figure 2). Since the TWI layer limits the development of cloud heights, the generated precipitation is predominated by warm rain from shallow cumulus clouds with a latent heating peak in the 1–3 km range [*Liu et al.*, 2015]. This condition is supported by a higher fraction of low and midlevel clouds from June to August 2013 in the study area (Figure 13d).

Thus, the $\delta^{18}O$ enrichment of rain during winter 2013 was due to the predominant strong shallow convection system that generated a greater amount of precipitation from relatively lower cloud heights and warmer temperatures, with mean altitudes of LH release between 1.5 and 4 km with corresponding temperatures between 5 and 18°C. In contrast, during summer 2013, a large-scale deep convection generated precipitation from higher and colder clouds with mean altitudes of LH release between 4 and 7 km, and with corresponding temperatures between −6 and 5°C, leading to the depletion of rainfall $\delta^{18}O$. The most enriched $\delta^{18}O$ was observed in September 2013 which was likely due to the formation of precipitation at lower and warmer clouds with maximum altitude of LH release at ~1.5 km and with a corresponding temperature of ~18°C (Figures 13b and 13c), while the low rainfall amount during this month (Figure 11, fourth panel) may have been due to the weakest latent heat release in 2013 (Figure 13a).

Unlike the lowland stations (PORT, TMK, and KK) that receive greater rainfall during the winter than the summer, TPR station shows little seasonality in precipitation (Figure 2). TPR (~1900 m asl) is located just below the TWI layer and is influenced by trade wind orographic showers during the winter. Therefore, the observed $\delta^{18}O$ upslope gradient at TPR from May to September 2013 was identical to the $\delta^{18}O$ upslope gradients at lowland stations (Figure 3). This may indicate that these stations have a similar gradient of mean condensation level of rainfall during this period as they are located below the TWI layer. On the other hand, the $\delta^{18}O$ upslope gradient at the highland GRS station is less steep, suggesting that rainfall was generated from higher (cooler) mean condensation levels (temperatures). This is likely because GRS is located above the TWI layer.

Scholl et al. [2009] provide information about the mean echo top altitudes and their associated atmospheric temperatures that were categorized by weather patterns [*Scholl et al.*, 2009, Table 3]. By applying this information, it could be inferred that the prevailing weather patterns during winter at GRS are dominated by troughs, thunderstorms, and easterly waves (tropical easterlies). For instance, showers with thunderstorms were often experienced by the BPCRC team during the ice core drilling operation on the Northwall Firn during June–July 2010. Furthermore, radiosonde records from New Guinea suggest that tropical easterlies are predominant and stronger from June to August at sea level up to at least 6000 m asl [*Permana*, 2011]. These observations support the conclusion that rainfall at GRS during winter 2013 likely resulted from higher (cooler) mean condensation levels (temperatures) than at other stations below the TWI layer.

6. Conclusions

This study directly evaluates the influence of precipitation amount and convective activity as well as the influence of condensation temperature on rainfall $\delta^{18}O$ in the southern part of the central mountain ranges of Papua where the precipitation amount and OLR values are positively correlated on seasonal timescales, in contrast to the typical relationship in the tropics. The influence of interannual ENSO variation is also examined by comparing rainfall stable isotopic compositions during the ENSO-normal and the El Niño periods in this region. Rainfall isotopic analyses indicate the nature of the altitude effect, with a mean isotopic lapse rate for $\delta^{18}O$ (δD) of −2.4‰/km (−18.2‰/km). Our analyses suggest that regional convective activity,

rather than local/regional precipitation amount and local surface temperature, is a more important factor for controlling rainfall $\delta^{18}O$ variability on daily to interannual timescales. Air mass back trajectories were simulated to discern the moisture sources and transport pathways. The findings also suggest that the spatio-temporal integrative effects of convective activity on rainfall $\delta^{18}O$ are more important than the rainout processes along the transport paths to the collection sites. The intraseasonal $\delta^{18}O$ variability at our sites resembles the large-scale MJO cycle, with major $\delta^{18}O$ depletion events associated with the active (wet) phases of the MJO. Furthermore, seasonal rainfall $\delta^{18}O$ is generally characterized by summer $\delta^{18}O$ depletion and winter $\delta^{18}O$ enrichment following the seasonal pattern of regional convective activity, but not precipitation. The regional convective activity is also the primary driver of monthly rainfall $\delta^{18}O$ variation within the ~2 year collection period. During the ENSO-normal period in 2013, the moisture sources, transport pathways, moisture convergence, and raindrop (secondary) evaporation appear to have had no significant seasonal effect on rainfall $\delta^{18}O$. This leads to the conclusion that on seasonal timescales the convection effect is likely associated with the temperature (at mean condensation level) effect. Mean condensation level is represented by the altitude of latent heat release in the troposphere. Therefore, the more depleted rainfall $\delta^{18}O$ during the summer is associated with enhanced deep convection such that precipitation is generated at higher (cooler) mean condensation levels (temperature). During the winter, local wind circulation is dominant, causing shallow convection which is limited by the TWI layer and results in greater precipitation amounts from lower (warmer) mean condensation levels (temperatures), eventually leading to more enriched rainfall $\delta^{18}O$. Thus, our results present another line of evidence pointing to the role of temperature on $\delta^{18}O$ in the tropics.

Rainfall $\delta^{18}O$ (δD) values at different elevation stations in Papua are generally enriched by 1.6‰–2‰ (11‰–15‰), and *d* values are lower at lower stations during El Niño than during ENSO-normal periods. Although these results are derived from only one ENSO cycle, they may provide empirical baseline information for further research on ENSO-$\delta^{18}O$ links on interannual timescales in tropical West Pacific. Finally, the analyses of climate controls on stable isotopes in precipitation from this study will be used to support the interpretation of the $\delta^{18}O$-based paleoclimate reconstruction from Papua ice cores that were drilled on glaciers near Puncak Jaya in 2010.

Acknowledgments

The authors would like to thank the anonymous reviewers for their valuable comments and suggestions to improve the quality of the manuscript. The authors also would like to thank Ping Nan Lin for stable isotope analysis and Mary Davis for revising and proofreading the manuscript. We also gratefully acknowledge the staffs from the environmental department of PTFI and the BMKG local office in Timika for providing meteorological data and collecting rain samples. The rain sampling program was conducted in conjunction with the ice core research program in the BPCRC at the Ohio State University, Research and Development Center of BMKG, and PTFI in Indonesia. Upon publication, data presented in this work will be archived at the National Oceanic and Atmospheric Administration (NOAA) World Data Center-A for Paleoclimatology: ftp://ftp.ncdc.noaa.gov/pub/data/paleo/icecore/trop/papua. This work was supported by National Science Foundation (NSF) grant ATM-0823586. This is a Byrd Polar and Climate Research Center contribution number 1539.

References

Aldrian, E., and R. Dwi Susanto (2003), Identification of three dominant rainfall regions within Indonesia and their relationship to sea surface temperature, *Int. J. Climatol.*, *23*(12), 1435–1452.

Arkin, P. A., and P. E. Ardanuy (1989), Estimating climatic-scale precipitation from space: A review, *J. Clim.*, *2*(11), 1229–1238.

Bosilovich, M. (2008), NASA's Modern Era Retrospective Analysis for Research and Applications: Integrating Earth Observations. [Available at www.earthzine.org/2008/09/26/nasas-modern-era-retrospective-analysis/.]

Breitenbach, S. F. M., J. F. Adkins, H. Meyer, N. Marwan, K. K. Kumar, and G. H. Haug (2010), Strong influence of water vapor source dynamics on stable isotopes in precipitation observed in southern Meghalaya, NE India, *Earth Planet. Sci. Lett.*, *292*(1–2), 212–220.

Buenning, N. H., L. Stott, K. Yoshimura, and M. Berkelhammer (2012), The cause of the seasonal variation in the oxygen isotopic composition of precipitation along the western U.S. coast, *J. Geophys. Res.*, *117*, D18114, doi:10.1029/2012JD018050.

Buenning, N. H., L. Stott, L. Kanner, and K. Yoshimura (2013), Diagnosing atmospheric influences on the interannual $^{18}O/^{16}O$ variations in Western U.S. precipitation, *Water*, *5*(3), 1116–1140.

Chen, Y., and A. J. Nash (1994), Diurnal variation of surface airflow and rainfall frequencies on the island of Hawaii, *Mon. Weather Rev.*, *122*(1), 34–56.

Christianto, D. (2014), Topography effects on rainfall variation at south Papua region MS thesis, Institut Teknologi Bandung, Indonesian.

Clark, I. D., and P. Fritz (1997), *Environmental Isotopes in Hydrogeology*, A. F. Lewis, New York.

Cobb, K. M., J. F. Adkins, J. W. Partin, and B. Clark (2007), Regional-scale climate influences on temporal variations of rainwater and cave drip water oxygen isotopes in northern Borneo, *Earth Planet. Sci. Lett.*, *263*(3–4), 207–220.

Craig, H. (1961), Isotopic variations in meteoric waters, *Science*, *133*(3465), 1702–1703.

Crawford, J., C. E. Hughes, and S. D. Parkes (2013), Is the isotopic composition of event based precipitation driven by moisture source or synoptic scale weather in the Sydney Basin, Australia?, *J. Hydrol.*, *507*, 213–226.

Dansgaard, W. (1964), Stable isotopes in precipitation, *Tellus*, *16*(4), 436–468.

Draxler, R. R., and Rolph, G. D. (2014), HYSPLIT (HYbrid Single-Particle Lagrangian Integrated Trajectory), Model access via NOAA ARL READY Website: http://www.arl.noaa.gov/HYSPLIT.php, last access: 27 December 2014, NOAA Air Resources Laboratory, College Park, Md.

Esteban, M. A., and Y. Chen (2008), The impact of trade wind strength on precipitation over the windward side of the island of Hawaii, *Mon. Weather Rev.*, *136*(3), 913–928.

Fudeyasu, H., K. Ichiyanagi, K. Yoshimura, S. Mori, J. Hamada, N. Sakurai, M. D. Yamanaka, J. Matsumoto, and F. Syamsudin (2011), Effects of large-scale moisture transport and mesoscale processes on precipitation isotope ratios observed at Sumatra, Indonesia, *J. Meteorol. Soc. Jpn. Ser. II*, *89A*, 49–59.

Gao, J., V. Masson-Delmotte, C. Risi, Y. He, and T. Yao (2013), What controls precipitation $\delta^{18}O$ in the southern Tibetan Plateau at seasonal and intra-seasonal scales? A case study at Lhasa and Nyalam, *Tellus B*, *65*, 21043, doi:10.3402/tellusb.v65i0.21043.

Gat, J. R., and E. Matsui (1991), Atmospheric water balance in the Amazon basin: An isotopic evapotranspiration model, *J. Geophys. Res.*, *96*(D7), 13,179–13,188, doi:10.1029/91JD00054.

Gonfiantini, R., M. Roche, J. Olivry, J. Fontes, and G. M. Zuppi (2001), The altitude effect on the isotopic composition of tropical rains, *Chem. Geol.*, *181*(1-4), 147–167.
Gu, G., and Zhang, C. (2002), Cloud components of the Intertropical Convergence Zone, *J. Geophys. Res.*, *107*(D21), 4565, doi:10.1029/2002JD002089.
Ichikawa, H., and T. Yasunari (2008), Intraseasonal variability in diurnal rainfall over New Guinea and the surrounding oceans during austral summer, *J. Clim.*, *21*(12), 2852–2868.
Jarvis, A., H. I. Reuter, A. Nelson, and E. Guevara (2008), Hole-filled SRTM for the globe version 4. [Available at the CGIAR-CSI SRTM 90 m database (http://srtm.csi.cgiar.org).]
Kurita, N. (2013), Water isotopic variability in response to mesoscale convective system over the tropical ocean, *J. Geophys. Res. Atmos.*, *118*, 10,376–10,390, doi:10.1002/jgrd.50754.
Kurita, N., K. Ichiyanagi, J. Matsumoto, M. D. Yamanaka, and T. Ohata (2009), The relationship between the isotopic content of precipitation and the precipitation amount in tropical regions, *J. Geochem. Explor.*, *102*(3), 113–122.
Kurita, N., D. Noone, C. Risi, G. A. Schmidt, H. Yamada, and K. Yoneyama (2011), Intraseasonal isotopic variation associated with the Madden-Julian Oscillation, *J. Geophys. Res.*, *116*, D24101, doi:10.1029/2010JD015209.
Lee, J., I. Fung, D. J. DePaolo, and C. C. Henning (2007), Analysis of the global distribution of water isotopes using the NCAR atmospheric general circulation model, *J. Geophys. Res.*, *112*, D16306, doi:10.1029/2006JD007657.
Lee, J., K. Johnson, and I. Fung (2009), Precipitation over South America during the Last Glacial Maximum: An analysis of the "amount effect" with a water isotope-enabled general circulation model, *Geophys. Res. Lett.*, *36*, L19701, doi:10.1029/2009GL039265.
Lekshmy, P. R., M. Midhun, R. Ramesh, and R. A. Jani (2014), ^{18}O depletion in monsoon rain relates to large scale organized convection rather than the amount of rainfall, *Sci. Rep.*, *4*, doi:10.1038/srep05661.
Liebmann, B., and C. A. Smith (1996), Description of a complete (interpolated) outgoing longwave radiation dataset, *Bull. Am. Meteorol. Soc.*, *77*, 1275–1277.
Liu, C., S. Shige, Y. N. Takayabu, and E. Zipser (2015), Latent heating contribution from precipitation systems with different sizes, depths, and intensities in the tropics, *J. Clim.*, *28*(1), 186–203.
Madden, R. A., and P. R. Julian (1972), Detection of a 40–50 day oscillation in the zonal wind in the tropical Pacific, *J. Atmos. Sci.*, *28*, 702–708.
Magagi, R., and A. P. Barros (2004), Estimation of latent heating of rainfall during the onset of the Indian monsoon using TRMM PR and radiosonde data, *J. Appl. Meteorol.*, *43*(2), 328–349.
McAlpine, J. R., G. Keig, and R. Falls (1983), *Climate of Papua New Guinea*, Commonwealth Scientific and Industrial Research Organization in Association with Australian National Univ. Press, Canberra, Aust.
Mechem, D. B., and A. J. Oberthaler (2013), Numerical simulation of tropical cumulus congestus during TOGA COARE, *J. Adv. Model. Earth Syst.*, *5*, 623–637, doi:10.1002/jame.20043.
Merlivat, L., and J. Jouzel (1979), Global climatic interpretation of the deuterium-oxygen 18 relationship for precipitation, *J. Geophys. Res.*, *84*, 5029–5033, doi:10.1029/JC084iC08p05029.
Moerman, J. W., K. M. Cobb, J. F. Adkins, H. Sodemann, B. Clark, and A. A. Tuen (2013), Diurnal to interannual rainfall $\delta^{18}O$ variations in northern Borneo driven by regional hydrology, *Earth Planet. Sci. Lett.*, *369*, 108–119.
Moore, M., Kuang, Z., and Blossey, P. N. (2014), A moisture budget perspective of the amount effect, *Geophys. Res. Lett.*, *41*, 1329–1335, doi:10.1002/2013GL058302, doi:10.1002/2013GL058302.
NASA (2011), MERRA: Modern Era Restrospective-Analysis for Research and Applications, Retrieved 07/08, 2011. [Available at http://gmao.gsfc.nasa.gov/merra/.]
Permana, D. (2011), Climate, precipitation isotopic composition and tropical ice core analysis of Papua, Indonesia, MS thesis, The Ohio State Univ., Columbus.
Poage, M. A., and C. P. Chamberlain (2001), Empirical relationships between elevation and the stable isotope composition of precipitation and surface waters: Considerations for studies of paleoelevation change, *Am. J. Sci.*, *301*(1), 1–15.
Prentice, M. L., and G. S. Hope (2007), Climate of Papua, in *The Ecology of Papua: Part One*, edited by A. J. Marshall and B. M. Beehler, pp. 177–195, Periplus Editions, Singapore.
Rhodes, A. L., A. J. Guswa, and S. E. Newell (2006), Seasonal variation in the stable isotopic composition of precipitation in the tropical montane forests of Monteverde, Costa Rica, *Water Resour. Res.*, *42*, W11402, doi:10.1029/2005WR004535.
Rienecker, M. M., et al. (2011), MERRA: NASA's Modern-Era Retrospective Analysis for Research and Applications, *J. Clim.*, *24*(14), 3624–3648.
Risi, C., S. Bony, F. Vimeux, L. Descroix, B. Ibrahim, E. Lebreton, I. Mamadou, and B. Sultan (2008a), What controls the isotopic composition of the African monsoon precipitation? Insights from event-based precipitation collected during the 2006 AMMA field campaign, *Geophys. Res. Lett.*, *35*, L24808, doi:10.1029/2008GL035920.
Risi, C., S. Bony, and F. Vimeux (2008b), Influence of convective processes on the isotopic composition ($\delta^{18}O$ and δD) of precipitation and water vapor in the tropics: 2. Physical interpretation of the amount effect, *J. Geophys. Res.*, *113*, D19306, doi:10.1029/2008JD009943.
Rozanski, K., Araguás-Araguás, L., and Gonfiantini, R. (1993), Isotopic patterns in modern global precipitation, in *Climate Change in Continental Isotopic Records*, *Geophys. Monogr. Ser.*, 78 ed., edited by P. K. Swart et al., pp. 1–36, AGU, Washington, D. C.
Salati, E., A. Dall'Olio, E. Matsui, and J. Gat (1979), Recycling of water in the Amazon basin: An isotope study, *Water Resour. Res.*, *15*, 1250–1258, doi:10.1029/WR015i005p01250.
Samuels-Crow, K. E., J. Galewsky, D. R. Hardy, Z. D. Sharp, J. Worden, and C. Braun (2014), Upwind convective influences on the isotopic composition of atmospheric water vapor over the tropical Andes, *J. Geophys. Res. Atmos.*, *119*, 7051–7063, doi:10.1002/2014JD021487.
Scholl, M. A., and T. B. Coplen (2010), Correlation between stable isotope composition and cloud altitude (radar echo tops) in tropical rainfall: Puerto Rico and Hawaii, Abstract A51E-0182 presented at 2010 Fall Meeting, AGU San Francisco, Calif.
Scholl, M. A., T. W. Giambelluca, S. B. Gingerich, M. A. Nullet, and L. L. Loope (2007), Cloud water in windward and leeward mountain forests: The stable isotope signature of orographic cloud water, *Water Resour. Res.*, *43*, W12411, doi:10.1029/2007WR006011.
Scholl, M. A., J. B. Shanley, J. P. Zegarra, and T. B. Coplen (2009), The stable isotope amount effect: New insights from NEXRAD echo tops, Luquillo mountains, Puerto Rico, *Water Resour. Res.*, *45*, W12407, doi:10.1029/2008WR007515.
Smith, T. M., R. W. Reynolds, T. C. Peterson, and J. Lawrimore (2008), Improvements to NOAA's historical merged land-ocean surface temperature analysis (1880–2006), *J. Clim.*, *21*(10), 2283–2296.
Sobel, A. H., I. M. Held, and C. S. Bretherton (2002), The ENSO signal in tropical tropospheric temperature, *J. Clim.*, *15*(18), 2702–2706.
Sukri, N. C., et al. (2003), Transmission of epidemic dengue hemorrhagic fever in easternmost Indonesia, *Am. J. Trop. Med. Hyg.*, *68*(5), 529–535.
Suwarman, R., K. Ichiyanagi, M. Tanoue, K. Yoshimura, S. Mori, M. D. Yamanaka, N. Kurita, and F. Syamsudin (2013), The variability of stable isotopes and water origin of precipitation over the maritime continent, *Sola*, *9*, 74–78.
Tao, W., et al. (2006), Retrieval of latent heating from TRMM measurements, *Bull. Am. Meteorol. Soc.*, *87*(11), 1555–1572.

Thompson, L. G., E. Mosley-Thompson, and K. A. Henderson (2000), Ice-core palaeoclimate records in tropical South America since the Last Glacial Maximum, *J. Quat. Sci.*, *15*(4), 377–394.

Thompson, L. G., E. Mosley-Thompson, M. E. Davis, P.-N. Lin, K. Henderson, and T. A. Mashiotta (2003), Tropical glacier and ice core evidence of climate change on annual to millennial time scales, *Clim. Change*, *59*(1–2), 137–155.

Tremoy, G., F. Vimeux, S. Mayaki, I. Souley, O. Cattani, C. Risi, G. Favreau, and M. Oi (2012), A 1-year long $\delta^{18}O$ record of water vapor in Niamey (Niger) reveals insightful atmospheric processes at different timescales, *Geophys. Res. Lett.*, *39*, L08805, doi:10.1029/2012GL051298.

Vimeux, F., G. Tremoy, C. Risi, and R. Gallaire (2011), A strong control of the South American seesaw on the intra-seasonal variability of the isotopic composition of precipitation in the Bolivian Andes, *Earth Planet. Sci. Lett.*, *307*(1–2), 47–58.

Vuille, M., Bradley, R. S., Werner, M., Healy, R., and Keimig, F. (2003), Modeling $\delta^{18}O$ in precipitation over the tropical Americas: 1. Interannual variability and climatic controls, *J. Geophys. Res.*, *108*(D6), 4174, doi:10.1029/2001JD002038.

Vuille, M., M. Werner, R. S. Bradley, and F. Keimig (2005), Stable isotopes in precipitation in the Asian monsoon region, *J. Geophys. Res.*, *110*, D23108, doi:10.1029/2005JD006022.

Windhorst, D., T. Waltz, E. Timbe, H. Frede, and L. Breuer (2013), Impact of elevation and weather patterns on the isotopic composition of precipitation in a tropical montane rainforest, *Hydrol. Earth Syst. Sci.*, *17*(1), 409–419.

Yoshimura, K., Oki, T., Ohte, N., and Kanae, S. (2003), A quantitative analysis of short-term ^{18}O variability with a Rayleigh-type isotope circulation model, *J. Geophys. Res.*, *108*(D20), 4647, doi:10.1029/2003JD003477.

Zhang, C., J. Ling, S. Hagos, W. Tao, S. Lang, Y. N. Takayabu, S. Shige, M. Katsumata, W. S. Olson, and T. L'Ecuyer (2010), MJO signals in latent heating: Results from TRMM retrievals, *J. Atmos. Sci.*, *67*(11), 3488–3508.

Zhou, L., and Y. Wang (2006), Tropical Rainfall Measuring Mission observation and regional model study of precipitation diurnal cycle in the New Guinean region, *J. Geophys. Res.*, *111*, D17104, doi:10.1029/2006JD007243.